AR-319-VOL-2

HYPERSONIC LAMINAR-TURBULENT TRANSITION

WILLIAM S. SARIC
Mechanical and Aerospace Engineering
Arizona State University
Tempe AZ 85287-6106 USA

ELI RESHOTKO
Mechanical and Aerospace Engineering
Case-Western Reserve University
Cleveland OH 44106 USA

DANIEL ARNAL
Départment Aérothermodynamique
ONERA / CERT
31055 Toulouse, FRANCE

ABSTRACT

The computational and experimental progress covering the four basic instability mechanisms that contribute to laminar-turbulent transition is reviewed. Streamwise, crossflow, centrifugal, and attachment-line instabilities and their principal means for initiating transition in hypersonic boundary layers are discussed. Comparisons between computations and experiments are given. Issues relating to how freestream disturbances influence the initial amplitudes of disturbances are also documented. Particular attention is paid to prediction schemes based on linear theory although other techniques are reviewed. This discussion is used to review the capabilities of present and future transition prediction methods as well as flow-quality requirements for hypersonic experimental facilities.

1 INTRODUCTION

The reliable computation of flowfields over hypersonic vehicles including skin friction and heat transfer information involves the determination of the location and extent of the region of laminar-turbulent transition. The rational estimation of transition location is generally not a part of any contemporary flowfield computational code. This report discusses some of the factors that would have to be considered in the estimation of transition behavior for hypersonic flight.

The evolution to turbulence in compressible boundary layers follows the generally accepted view that laminar-turbulent transition is a consequence of the nonlinear response of the laminar boundary layer to forcing disturbances. These disturbances are part of the environment within which the laminar flow develops and could include freestream turbulence, entropy disturbances, radiated sound, surface roughness, surface vibrations, etc., or any combination of these. These freestream disturbances enter the boundary layer as steady and/or unsteady fluctuations of the basic state. This part of the process is called *receptivity* (Morkovin, 1969) and although it is still not well understood, it provides the vital initial conditions of amplitude, frequency, and phase for the breakdown of laminar flow. Initially these disturbances may be too small to measure and they are observed only after the onset of an instability. A variety of different instabilities can occur independently or together and the appearance of any particular type of instability depends on Reynolds number, wall curvature, sweep, roughness, and initial conditions. The initial growth of these disturbances is described by *linear* stability theory (i.e. linearized, unsteady, Navier-Stokes). This growth is weak, occurs over a viscous length scale, and can be modulated by pressure gradients, surface mass transfer, temperature gradients, etc. As the amplitude grows, three-dimensional and nonlinear interactions occur in the form of *secondary* instabilities. Disturbance growth is very rapid in the case (now over a convective length scale) and breakdown to turbulence occurs.

Since the linear stability behavior can be calculated, transition prediction schemes are usually based on linear theory. However, since the initial conditions (receptivity) are not generally known, only correlations are possible and, most importantly, these corrections must be between two systems with similar environmental conditions.

At times, the initial instability can be so strong that the growth of linear disturbances is *by-passed* (Morkovin, 1969) and turbulent spots or secondary instabilities occur and the flow quickly becomes turbulent. This phenomenon is not well understood but has been documented in cases of roughness and high freestream turbulence (Reshotko, 1986). In this case, transition prediction schemes based on linear theory fail completely.

In the flight environment without large surface roughness, the most successful of the transition estimation techniques are those based on the results of linear stability calculations. Presently we have only developing knowledge of the nonlinear phenomena and breakdowns at supersonic and hypersonic speeds. Thus, much of what is discussed herein relies on linear theory.

This paper has benefited from other recent reviews of the important issues, principally those of Morkovin (1987, 1988), Morkovin and Reshotko (1990), Reed and Saric (1989), Reshotko (1994), and Reed et al. (1996, 1997). In particular, the work of Reed et al. (1997) directly complements this report.

2 GENERAL BACKGROUND

2.1 Linear Stability Theory

Linear theory addresses the first stage of boundary-layer eigenmode development, both for two-dimensional (2D) and three-dimensional flows (3D) The most thorough review of the details of the theory is given by Mack (1984). The principle is to introduce small sinusoidal disturbances into the Navier-Stokes equations in order to compute the range of unstable frequencies. Linear stability theory can be used either in its *local* or in its *nonlocal* formulation.

2.1.1 Local Formulation

Any fluctuating quantity r' (velocity, pressure, density or temperature) is expressed by:

$$r' = r(y) \quad \exp[i(\alpha x + \beta z - \omega t)] \tag{1}$$

where x, y, z is an orthogonal coordinate system, which can be either Cartesian or curvilinear, y being normal to the surface. The complex amplitude function r depends on y only. In the general case, α, β, and ω are complex numbers.

The fluctuating quantities are very small, so that the quadratic terms of the disturbances can be neglected in the Navier-Stokes equations. It is also assumed that the mean flow quantities do not vary significantly over a wavelength of the disturbances; therefore U and W (mean flow components in the x and z directions) as well as the mean temperature T are functions of y alone, and the normal velocity V is equal to zero. The implication of this *parallel flow approximation* is that the stability of the flow at a particular station (x, z) is determined by the local conditions at that station independently of all others.

This leads to a system of homogeneous, ordinary differential equations for the amplitude functions $r(y)$. The homogeneous boundary conditions (the disturbances must vanish in the freestream and the velocity fluctuations are zero at the wall), establish an eigenvalue problem: when the mean flow is specified, nontrivial solutions exist only for certain combinations of the parameters α, β, ω and R, where R is the Reynolds number. This constitutes the *dispersion relation.*

In this paper, the discussion will be restricted to the *spatial theory*, which is more relevant than the temporal theory for boundary-layer flows. Thus, ω is real, α and β are complex: $\alpha = \alpha_r + i\alpha_i$ and $\beta = \beta_r + i\beta_i$. Then r' is expressed by:

$$r' = r(y) \quad \exp(-\alpha_i x - \beta_i z) \quad \exp[i(\alpha_r x + \beta_r z - \omega t)] \tag{2}$$

It is possible to define a wavenumber vector $\vec{k} = (\alpha_r, \beta_r)$ and an amplification vector $\vec{A} = (-\alpha_i, -\beta_i)$ with angles φ and $\bar{\varphi}$ with respect to the x direction:

$$\varphi = \tan^{-1}(\beta_r / \alpha_r) \tag{3}$$

$$\bar{\varphi} = \tan^{-1}(\beta_i / \alpha_i) \tag{4}$$

From these definitions, it is now clear that any eigenvalue problem involves six real parameters $(\alpha_r, \alpha_i, \beta_r, \beta_i, \omega, R)$ which are often replaced by $(\alpha_r, \alpha_i, \varphi_r, \bar{\varphi}_i, \omega, R)$. The input data are the mean velocity and mean temperature profiles and four of the six parameters listed above. The computation gives the values of the two remaining parameters (eigenvalues) as well as the disturbance amplitude profiles (eigenfunctions).

2.1.2 Nonlocal Formulation

A new formulation for the stability analysis was recently proposed by Herbert (see overview in Herbert 1994) and by DLR Göttingen (see Simen and Dallmann 1992 and Dallmann et al. 1996). In this approach, the general expression of the disturbances is:

$$r' = r(x, y) \quad \exp[i(\theta(x) + \beta z - \omega t)] \text{ with } \frac{d\theta}{dx} = \alpha(x) \tag{5}$$

α is complex, β and ω are real and constant. In contrast to the local approach expressed by relation (1), the amplitude functions depend on y and x, and α depends on x. Substituting the previous expression into the stability equations, neglecting $\partial^2 r / \partial x^2$ and linearizing in r yield a partial differential equation of the form:

$$Lr + M\frac{\partial r}{\partial x} + \frac{d\alpha}{dx}Nr = 0 \qquad (6)$$

where L, M, and N are operators in y with coefficients that depend on x and y through the appearance of the basic flow profiles and of the wavenumber α. When $d\alpha/dx$ is computed from a so-called normalization condition, the previous equation can be solved using a marching procedure in x with prescribed initial conditions: this constitutes the PSE (Parabolized Stability Equations) approach. The interest of this procedure is that the nonparallel effects are taken into account. As it will be discussed in section 2.2, it is also possible to introduce the *nonlinear* terms.

2.2 Nonlinear Approaches

Today, several approaches are available to analyze the behavior of the disturbances when they begin to deviate from the linear amplification regime. These numerical tools include, for instance, the method of multiple scales or the secondary instability theories (Herbert 1988). DNS are of course particularly helpful for improving the understanding of the nonlinear mechanisms. For practical applications, nonlinear PSE are particularly attractive; although they only describe *weakly nonlinear phenomena*, they are less time-consuming than DNS and they can be used for rather complex geometries.

The basic ideas of the nonlinear PSE have been explained in many papers, see for instance Herbert (1994) and Reed et al. (1998). The disturbances are written as double Fourier expansions containing two- and three-dimensional discrete normal modes denoted as (n, m) modes:

$$r' = \sum_{n=\infty}^{\infty}\sum_{m=\infty}^{\infty} r_{n,m}(x,y)F_{n,m} \qquad (7)$$

with

$$F_{n,m} = \exp\left[i\left[\int_{x_0}^{x}\alpha_{n,m}(\xi)d\xi + m\beta z - n\omega t/2\right]\right]$$

$\alpha_{n,m}$ is complex, β and ω are real and constant. Introducing (7) into the Navier-Stokes equations leads to a system of coupled partial differential equations which are solved by a marching procedure in the x direction. This method makes it possible to treat nonlinear mode interactions with a numerical effort which is much less than that required by DNS.

3 STATE-OF-THE-ART CONSIDERATIONS

3.1 Streamwise Instability

Theoretical studies have concentrated principally on determining the character and properties of the growing normal modes. In their pioneering study, Lees and Lin (1946) introduced the generalized inflection criterion (maximum of the local angular momentum $\rho\partial U/\partial y$), and the classification of disturbances as subsonic or supersonic with respect to the local external flow. Subsonic disturbances whether neutral, growing, or decaying all display exponential drop-off of amplitude at large distances from the wall. The neutral stability curves of the subsonic modes in the inviscid limit for insulated, flat-plate compressible boundary layers are described in Fig. 1 (Mack 1969). The lowest mode (n = 1) is the vortical mode which corresponds to the TS modes of the subsonic boundary layer. The higher subsonic modes ($n \geq 2$), discovered by Mack (1965a), are trapped acoustic modes that occur when additionally the wall is supersonic relative to the phase velocity $(c_r/a_w > 1)$. For insulated surfaces, these higher "Mack" modes appear for $M > 2.2$; however it is not until the Mach number is of the order of 4 or greater that the second mode is at a low enough frequency to have experimental consequences as shown in Fig. 2. Once the second mode sets in, it becomes the dominant instability since its growth rate tends to exceed that of the first mode. For insulated surfaces this occurs for $M > 4$ as shown in Fig. 3. For cooled surfaces, second-mode dominance can occur at even lower Mach number. In contrast to the first or TS mode, the higher subsonic modes are destabilized by cooling (Mack 1969). Indications are that the second-mode subsonic disturbances can be somewhat stabilized by favorable pressure gradient or by suction (Malik 1988, Malik 1989, Mack 1990a).

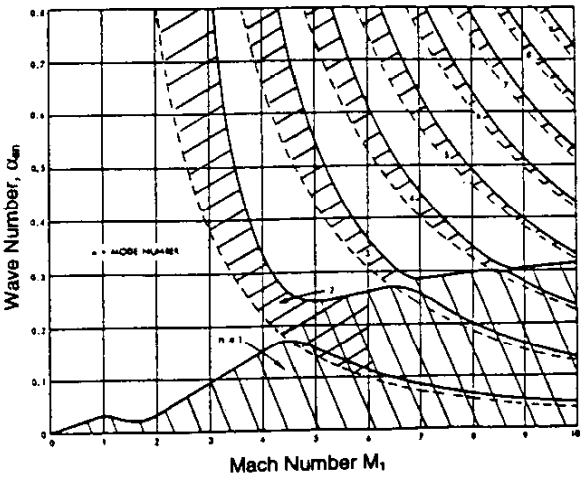

Figure 1. Wave numbers $2\pi L^*/\lambda^*$ corresponding to inviscid compressible instabilities in insulated flat-plate boundary layers. (2D Waves). Solid lines are subsonic waves. Dashed lines are supersonic waves. (Mack 1969).

Supersonic disturbances $(c_r < 1 - 1/M_e)$ were long considered irrelevant since supersonic neutral disturbances have non-vanishing amplitudes at infinite distances from the wall. Mack (1969) has shown, however, that amplifying outgoing supersonic disturbance amplitudes do decay exponentially for large y, albeit slowly, and are therefore acceptable normal modes.

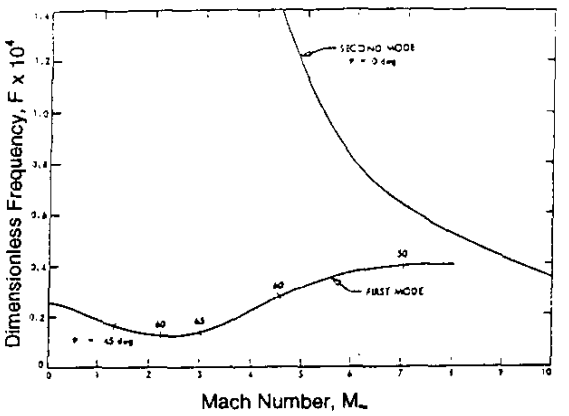

Figure 2. Effect of Mach number on first-and second-mode most unstable frequencies $Re = 1500$, insulated wall; wind tunnel temperatures (Mack 1969).

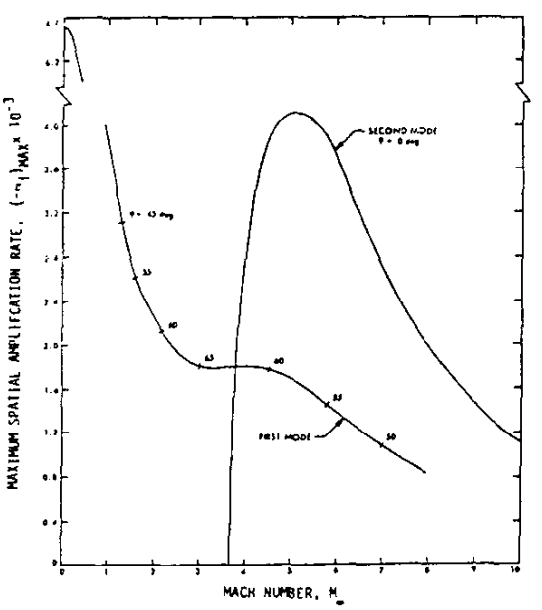

Figure 3. Effect of Mach number on spatial amplification rate of most unstable first-and second-mode disturbances $Re = 1500$. Insulated wall; wind tunnel temperatures (Mack 1969).

Mack (1969) found second-mode supersonic disturbances at $M = 5.8$ for highly-cooled walls $(T_w/T_{aw} < 0.15)$ in the inviscid limit. Their growth rates however were found to be much lower than those of the subsonic disturbances and their wavenumbers (frequencies) noticeably larger. Mack (1990a) has also calculated cases of highly-cooled boundary layers at $M = 3$ and $M = 4.5$, again in the inviscid limit, and found second-mode supersonic disturbances that are destabilized by suction. Although the growth rates of these latter disturbances approach the levels associated with subsonic disturbances, the disturbance wavenumbers and corresponding frequencies are very large. The significance of these disturbances to the transition process is likely to be negligible since Mack (1990b) further indicates that they are strongly damped at finite Reynolds number.

3.1.1 Description of Mack Modes

As stated above, the Mack modes are trapped acoustic modes whose phase velocities are subsonic with respect to the freestream but supersonic with respect to the wall. Their geometry was clarified by Morkovin (1987). Referring to Fig. 4, harmonic vorticity and entropy perturbations traveling along y_1 (the height of the sonic speed relative to y_s) are shown to be phase-tuned to coupled trapped acoustic perturbations traveling to the wall and back along Mach lines, stationary in this frame of reference. The reflection at the sonic streamline changes compression to expansion and vice-versa (the essence of the trapping). As a geometrical consequence, perfect phase coincidences at any Mach number occur only for wave number α_{1n} in the exact ratios to α_{11} of 1, 3, 5, ... 2n-1. This is the property of Mack's noninflectional neutral-mode families as shown as dotted lines in Fig. 1.

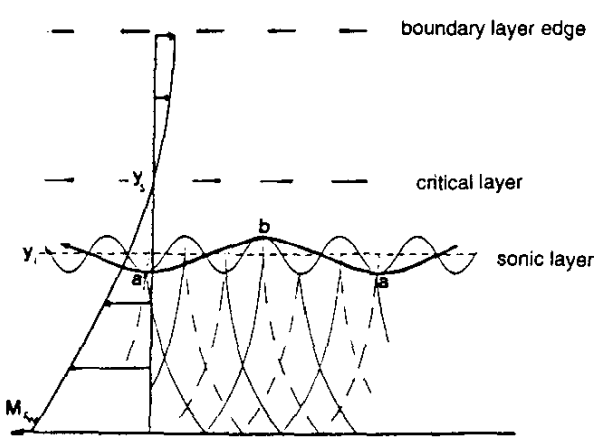

Figure 4. View of the mean flow and of vorticity-entropy-pressure disturbance interactions along characteristic curves in higher instability modes, (Mack modes) as seen when traveling with the flow at the height of the generalized inflection point.

3.1.2 e^N Method

The so-called e^N method is widely used by people who are assigned the job of making transition prediction. It was first developed by Smith and Gamberoni (1956) and by van Ingen

(1956) for low-speed flows and then extended to compressible and/or three-dimensional flows.

The e^N method is based on linear theory only, so that many fundamental aspects of the transition process are not accounted for. However, one has to keep in mind that there is no other practical method presently available for industrial applications. Caveats regarding the use and application of this method are found in Morkovin and Reshotko (1990).

Incompressible flows. In this case, only 2D waves $(\beta = 0)$ are considered. The disturbances are amplified or damped according to the sign of the spatial growth rate $-\alpha_i$.

For a given mean flow, it is possible to compute the total amplification rate of a spatially growing wave by integrating the local growth rate in the streamwise direction:

$$\ln(A/A_0) = \int_{x_0}^{x} -\alpha_i dx \tag{8}$$

where A is the wave amplitude and the index 0 refers to the streamwise position where the wave becomes unstable. The envelope of the total amplification curves is:

$$N = \max_f [\ln(A/A_0)] \tag{9}$$

In incompressible flow, with a low disturbance environment, experiments show that transition occurs when the *N-factor* reaches a critical value in the range 7—10, i.e., when the most unstable wave is amplified by a factor e^7 to e^{10}.

Compressible flows. When compressibility begins to play a role, the problem becomes more complex, because the most unstable waves are often oblique waves. As a consequence, a new parameter enters the dispersion relation: the angle φ between the streamwise direction and the wavenumber vector. It is still assumed that the amplification takes place in the x-direction only, i.e., $\beta = 0$ or $\overline{\varphi} = 0$, but β_r (or φ) needs to be specified.

For *second-mode disturbances*, the problem is rather simple, because the most unstable direction is $\varphi = 0°$ i.e., $\beta_r = 0$. As β_i is also zero, it is sufficient to drop βz in the exponential term of equation (1).

For *first-mode disturbances*, the most unstable direction is no longer the x-direction; in addition, this direction varies when the computation proceeds downstream. Two strategies are essentially used for two-dimensional flows:

- At each streamwise location, one finds the direction, φ_M, of the wave which gives the maximum value $-\alpha_{iM}$ of α_i. The *N-factor* is then defined by:

$$N = \max_f \int_{x_0}^{x} -\alpha_{iM} dx \tag{10}$$

  This is the so-called *envelope method.*

- The integrations are performed by following waves having a given dimensional frequency f and a constant value of the dimensional component β_r of the wavenumber vector in the spanwise direction. The *N-factor* is then computed by maximizing the total growth rate with respect to both f and β_r. The interest of this *fixed-frequency/fixed-spanwise-wavenumber method* is that it is congruent with the expression of the disturbances in the nonlocal theory.

Examples of application. The results presented in this section have been obtained with the local approach. Additional details are given in Reed et al. (1996, 1997). Comparison between local and nonlocal results will be discussed later on.

In supersonic and hypersonic wind tunnels, the main factor affecting transition on the models is noise, the origin of which lies in the pressure disturbances radiated by the turbulent boundary layers developing along the nozzle walls. This leads to low transition Reynolds numbers, i.e., small values of the *N-factor* at transition; typical values are in the range between 1 and 4.

Since the radiated noise is inherent in the presence of walls around the model, there is little doubt concerning the incapacity of conventional ground facilities to properly simulate free-flight conditions. In order to reduce this noise level, it is necessary to delay transition on the nozzle walls because a laminar boundary layer is less noisy than a turbulent one. This was done in the *quiet tunnel* built at NASA Langley with a freestream Mach number $M_\infty = 3.5$ (see description in Beckwith 1983). Notable features are the use of boundary-layer bleed slots upstream of the throat, a careful polishing and a careful design of the nozzle walls contour in order to minimize the development of Görtler vortices. With a laminar boundary layer on the nozzle walls, the measured pressure fluctuations can be one or two orders of magnitude below those measured in conventional facilities.

Several transition experiments were carried out in the quiet tunnel. On a flat plate, transition Reynolds numbers R_{XT} as high as 12×10^6 were measured; this result corresponds to *N-factors* around 10 (Chen and Malik 1988). The flow on supersonic sharp cones constitutes a second case where the freestream Mach number is constant in the streamwise direction. Measurements performed in the quiet tunnel give values of R_{XT} close to 7 or 8×10^6. The predicted transition Reynolds number computed for $N = 10$ is 8×10^6, in good agreement with experimental data (Chen and Malik 1988).

The problem is to know whether or not low-disturbance-level wind tunnels are representative of free-flight conditions. As

direct comparisons of the disturbance environment are difficult to perform, indirect comparisons are made by looking at the value of the *N-factor* at transition. In this respect, the flight experiments on the so-called AEDC cone (Fisher and Dougherty 1982) provided us with some interesting information. Malik (1984) computed the *N-factor* for four flight-test points corresponding to $M_\infty = 1.2$, 1.35, 1.6 and 1.95. He found transition Reynolds numbers at the onset of transition that were correlated by *N-factors* between 9 and 11.

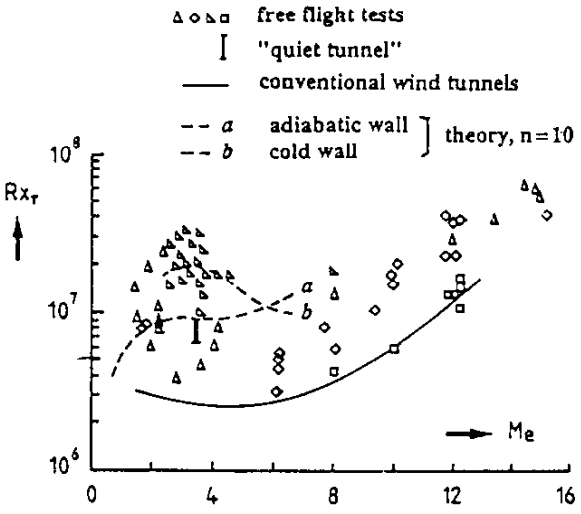

Figure 5.Comparison between measured and predicted transition Reynolds numbers on sharp cones

Unfortunately, reliable and accurate free flight data are scarce at higher, hypersonic Mach numbers. Figure 5 shows flight transition results collected for sharp cones by Beckwith (1975). The transition Reynolds numbers R_{XT} are plotted as function of the freestream Mach number. The figure also contains a correlation for wind tunnel transition data, which lies much below the flight results. The range of R_{XT} measured in the quiet tunnel are reported for comparison. The main reason for the large scatter in the free-flight results is that these data have been obtained for various conditions of wall temperatures, the distribution of which is not known in many cases. Malik (1989) calculated the values of R_{XT} corresponding to $N = 10$ for a 5° half angle cone and for Mach numbers up to 7. He made two series of computations: one by assuming that the wall was adiabatic, and the other by assuming that the wall temperature decreased with increasing M_∞ according to a certain empirical relationship. The latter computations (curve *b* in Fig. 5) make it possible to reproduce the trends exhibited by the flight results.

The e^N method was also used by Malik et al. (1990b) for the rather complex reentry-F experiments. The reentry-F vehicle (Johnson et al. 1972) consisted of a 5° half angle cone with an initial nose radius of 2.54 mm. Computations were performed at an altitude corresponding to a freestream Mach number close to 20. The basic flow was calculated by equilibrium gas Navier-Stokes and PNS codes. At the measured transition location, the *N-factor* was around 7.5. Roughness effects probably affected the transition mechanisms, so that the value of N would be somewhat larger for a perfectly smooth surface.

The conclusion is that the e^N method with $N \cong 10$ can be applied to predict transition in high-speed two-dimensional flows if the background disturbance level is low enough and if the wall is smooth.

Examples of parametric studies: Bluntness effects. Even if the exact value of the *N-factor* is not known for practical applications, the e^N method remains a very efficient tool for parametric studies: for a given test model and for a given disturbance environment, it is often able to predict the variation of the transition location as a function of the variation of a key parameter which governs the stability properties of the mean flow.

In hypersonic flows, the nose bluntness of a cone at zero angle of attack strongly affects the transition location. For instance, Malik et al. (1990a) performed a linear stability analysis for the experimental conditions studied by Stetson et al. (1984). In these experiments $(M_\infty = 8)$ the transition mechanisms were investigated on a cone which could be equipped with interchangeable spherically blunted noses of various radii. By using the e^N method, Malik et al. found that the predicted transition Reynolds number increased due to small nose bluntness, in qualitative agreement with experimental results. They also demonstrated that nose bluntness could explain the unit Reynolds number effect observed in the aeroballistic range data of Potter (1974).

Quite recently, ESA (European Space Agency) launched a TRP (Technological Research Programme) involving several research centers under the responsibility of Aerospatiale. The general objective was to analyze laminar-turbulent transition problems for hypersonic flow on slender lifting configurations. One of the experimental studies was devoted to the effect of nose bluntness for a cone placed at zero angle of attack in a wind tunnel at Mach 7 (unit Reynolds number $= 25 \times 10^6/\text{m}$). It was found that the e^N method was able to reproduce the rearward movement of the transition point when the nose radius increased from (nearly) 0 to 0.5 mm; the chosen value of the *N-factor* was that corresponding to the sharp cone case (Tran et al. 1995; Arnal et al. 1996).

3.1.3 Stability and Transition Experiments at Hypersonic Speeds

Meaningful stability and transition experiments at hypersonic speeds require facilities or techniques that are free of influence of the noise content of the facility. The stability experiments are best performed by inputting prescribed disturbances and measuring their growth properties. Of course, through astute signal analysis, the growth of tunnel disturbances can also be monitored and stability characteristics deduced, but there can be aliasing problems. Of the stability experiments performed before 1990, most notable are the $M = 4.5$ flat-plate experiment of Kendall (1975) and the cone experiments of Stetson et al (1991) in AEDC Tunnel B summarized by Stetson and Kimmel (1992). By inputting 2D and oblique disturbances, Kendall mapped out the first- and second-mode stability characteristics of the adiabatic flat-plate boundary layer. Stetson et al. (1991) did not generate disturbances in the boundary layer but relied on an analysis of the response of the boundary layer to the disturbance content in the wind tunnel. Transition experiments on the other hand should be done in quiet tunnels, which hardly exist at hypersonic speeds. Conventional tunnels above Mach 8 or so tend to have very low noise levels at second mode and higher frequencies and so have been used to obtain transition data. But since such tunnels are not quiet at subharmonic and mode-mode interaction frequencies, the nonlinear interactions leading to transition can be different than in flight. The discussion in this section will emphasize work performed in the last five years.

Experiments in the $M = 5$ Ludwieg Tube Facility at DLR. A set of flat-plate and cone experiments have been performed in the $M = 5$ Ludwieg-tube facility at DLR (Wendt et al. 1993, Krogmann 1996). The authors claim that despite having turbulent nozzle-wall boundary layers, this facility is quieter than conventional supersonic tunnels but not as quiet as the $M = 3.5$ quiet tunnel at NASA-Langley (Beckwith et al 1983) or the new quiet-flow Ludwieg tube facility at Purdue University (Schneider and Haven 1995). Although not specified, the ratio T_w/T_{aw} is estimated to be about 0.9 for all these tests. Based on analysis of the response in the boundary layer to tunnel disturbances, the authors conclude that their signals are primarily from growing oblique first-mode disturbances. They could not find any significant second-mode response in their tests. They accordingly conclude that transition in their facility is first-mode dominated and are surprised by this result. They should however not have been surprised. In an e^N study of transition on sharp cones at zero angle-of-attack, Malik (1989) showed that for adiabatic walls, the transition is first-mode dominated up to $M_\infty \approx 7$, and second-mode dominated above that. Thus there is no inconsistency between the $M_\infty = 5$ results at DLR and second-mode dominant experiments of Stetson et al. (1991) at $M_\infty = 8$. The $M_\infty = 5$ condition is not hypersonic enough for second-mode dominance. The transition Reynolds numbers (Krogmann 1996), are of course lower than the expected values from e^N calculations since the facility is not sufficiently quiet. But they are remarkably independent of unit Reynolds number.

Experiments at $M = 8$ in AEDC Tunnel B. As a follow-on to the circular cone experiments at $M_\infty = 7.93$ in AEDC Tunnel B reported by Stetson and Kimmel (1992), there have been recent measurements reported (Kimmel et al. 1996; Kimmel and Poggie 1997; Poggie and Kimmel 1997) that address the three-dimensional structure of the instability waves. It was earlier established that the initial instability is second mode and its growth is in accordance with linear theory. Using two hot-film probes, both located at the height in the boundary layer of maximum broadband rms signal, but with varying circumferential separation, the correlation of the signals (Fig. 6) indicates second-mode disturbances (streamwise wavelength $\sim 2\delta$) that are essentially two-dimensional.

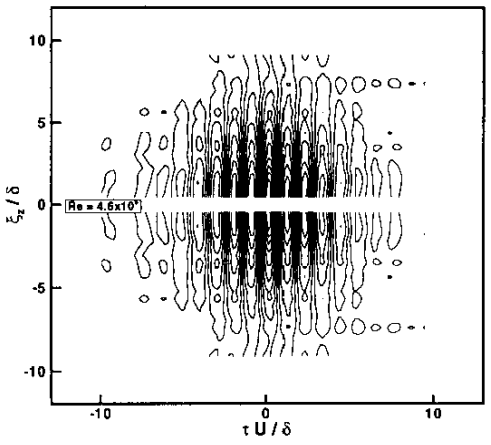

Figure 6. Circumferential correlations on the axisymmetric cone for $Re_x = 2.3\times10^6$ (Kimmel and Poggie 1997).

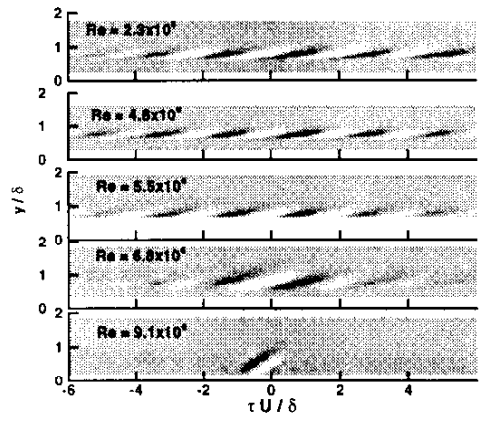

Figure 7. Vertical correlations on the axisymmetric cone.

Correlations in the vertical direction were obtained using two probes separated vertically by 1.47 mm and traversing them vertically through the boundary layer. With appropriate signal analysis (see Kimmel and Poggie 1997), the second-mode waves are shown to have a flattened structure (Fig. 7) that agrees qualitatively with shadowgraphs of the "rope waves" for the same configuration. These rope waves which appear before boundary-layer breakdown, seem to be a nonlinear manifestation of the second mode. With an increase in Reynolds number approaching transition, the waves become more erect approaching the angles of turbulent structures.

Cone experiments at $M = 5$ in the Caltech T5 Hypervelocity Shock Tunnel. Boundary-layer transition experiments were performed on a 5° half-angle cone at zero angle-of-attack in air, nitrogen and carbon dioxide (Germain et al. 1993; Adam and Hornung 1997). With air and nitrogen as test gases, reservoir enthalpies varied from 4 MJ/kg to 27 MJ/kg at stagnation pressures from 10 MPa to 85 MPa. For carbon dioxide, reservoir enthalpies varied from 3 MJ/kg to 10 MJ/kg and reservoir pressures from 40 MPa to 95 MPa. Dissociative effects are clearly important. The wall temperature is not specified. However, assuming it to be about 300 K gives a wall enthalpy of just under 0.6 MJ/kg for air and nitrogen and just under 0.5 MJ/kg for carbon dioxide. So these tests are conducted under very cold-wall conditions where under linear stability arguments, the second mode should dominate.

However, while the disturbance environment is not quantitatively described, it is generally regarded as noisy. Therefore the relationship between the obtained results and linear stability arguments is not clear. Adam and Hornung (1997) state that no clear relationship is found to exist between the transition Reynolds number based on the boundary layer edge conditions and the reservoir enthalpy. However, when reference temperature conditions are used instead, the different test gases give distinguishable results which are ordered according to their dissociation energies. These authors also compare their T-5 results with Reentry-F flight data reported by Wright and Zoby (1977). The flight data are in a Mach number range from about 8 to 20 and are taken in a relatively quiescent environment. Nevertheless, Adam and Hornung (1997) show that the transition Reynolds numbers under reference temperature conditions are between 600,000 and 2,000,000 for both the T-5 and the Reentry-F flight data. This collapse of data is interesting and unexpected. More data are needed to show that this result is other than fortuitous.

Stability experiments on a flared cone model in the NASA-Langley Mach 6 Quiet Tunnel. Experiments were conducted on 5° half-angle cones followed by large-radius circle-arc flares. The experiments at adiabatic wall conditions with and without small bluntness are by Lachowitz et al. (1996). Those on the sharp-tipped model at small angles of attack are by Doggett et al. (1997), while those on a slightly different sharp-tipped model with wall cooling are by Blanchard (1995). All three sets of experiments are summarized by Wilkinson (1997). In all cases, the cone portions of the models and a portion of the flare region were free from any tunnel noise. Only the aft portions of the flare were subject to low-level radiated noise from the part of the nozzle wall boundary layers that were undergoing some mild Görtler instability growth. The experiments included a detailed study of the mean flow and the stationary freestream disturbance patterns in the Mach 6 nozzle. The experiments documented the growth of the dominant second-mode disturbances with adverse pressure gradient, small nose bluntness, wall cooling and small angle of attack.

Under adiabatic wall conditions, the recovery temperature distributions on the sharp-tipped model showed transition occurring only at the very end of the flared section. Hot-wire spectra for this case taken at each streamwise measuring station showed a dominant second-mode peak at about 226 kHz corresponding to a linear stability prediction of 230 kHz (Balakumar and Malik 1994). There are however also harmonic peaks around 449 kHz and 670 kHz indicating some nonlinear behavior. Very small nose bluntness eliminated transition but still showed some growth of the second mode at around 230 kHz. With slightly larger nose bluntness there was neither transition nor evidence of second-mode growth. At two degrees angle of attack, the boundary layer on the windward side is stabilized and the dominant second-mode frequency increased, while on the leeward side the boundary layer is destabilized and the dominant frequency sharply decreased. Also on the leeward side, localized peaks over a range of low frequencies are observed upstream of the second-mode growth. These may be associated with crossflow instability.

Under cold wall conditions (sharp-tipped model at zero angle of attack), the second-mode frequency is at slightly higher frequency as expected theoretically (Balakumar and Malik 1994), the first harmonic (at just under 600 kHz) is comparable in amplitude to the fundamental and transition is advanced to mid-flare.

Transition studies on curved compression surfaces in the Calspan 48-inch Hypersonic Shock Tunnel. Pressure and heat transfer measurements were made on a curved compression ramp whose geometry is typical of an inlet to a scramjet engine (Holden and Chadwick 1995). The measurements were made at Mach numbers 10, 11 and 12 for a range of Reynolds numbers at each Mach number to place the beginning of transition at various stations along the ramp. Whereas the thin-film heat flux gauges were capable of obtaining transient data,

and these were used to more closely identify transition locations, only mean heat transfer data are presented. In the absence of spectral information, it is not possible to identify the dominant modes of the pre-transitional growth.

The transition results are not particularly sensitive to the small differences in Mach number in the $M = 10 - 12$ range. At the highest unit Reynolds numbers, transition occurs on the 5" wedge preceding the curved portion of the ramp. As unit Reynolds number is lowered, transition moves downstream as expected until at the lowest unit Reynolds numbers tested, it occurs around the end of the curved ramp. Although transition Reynolds numbers are not computed, it appears that the highest transition Reynolds numbers are obtained at the highest unit Reynolds numbers. Some of the reduction in transition Reynolds number with unit Reynolds number is due to the influence of the adverse pressure gradient on the compression ramp, and in fact, the length of the transition zone is reduced when the transition occurs on the curved ramp. In these experiments the maximum end-of-transition Reynolds number is about 3×10^6, below what one expects in flight at these Mach numbers. The facility may not be "quiet" enough for flight-quality data for the reported tests.

3.1.4 Effects of Chemistry and Bow Shock (Reed et al. 1997)

Linear stability solutions for hypersonic flows are complicated for some of the following reasons. 1) At hypersonic speeds, the gas often cannot be modeled as perfect because the molecular species begin to dissociate due to aerodynamic heating. In fact, sometimes there are not enough intermolecular collisions to support local chemical equilibrium and a nonequilibrium-chemistry model must be used. 2) The bow shock is close to the edge of the boundary layer and must be included in studies of transition.

Malik (1987, 1989, 1990) investigated the stability of an equilibrium-air boundary layer on an adiabatic flat plate. Malik et al. (1990) used the e^N method for the reentry-F experiments; the basic state was calculated by equilibrium-gas Navier-Stokes and PNS. Gasperas (1990) studied stability for an imperfect gas. Stuckert and Reed (1994) analyzed the stability of a shock layer in chemical nonequilibrium and compared results with the flow assuming 1) local chemical equilibrium and 2) a perfect gas.

Stuckert and Reed's coordinate system for both the basic-state and stability analysis fit the body and bow shock as coordinate lines. This makes it easier to apply the linearized shock-jump conditions as the disturbance boundary conditions (e.g. Stuckert 1991). At the surface of the cone, for the nonequilibrium calculations, the species mass fluxes were set to zero (non-catalytic wall), whereas for the equilibrium calculations the disturbances were assumed to be in chemical equilibrium. It is clear that the equilibrium and nonequilibrium solutions can differ significantly depending on the rates of the reactions relative to the time scales of convection and diffusion. For example, some of the equilibrium modes were determined to be supersonic modes, each of which was a superposition of incoming and outgoing amplified solutions in the inviscid region of the shock layer. (No similar solutions were found for the nonequilibrium shock layer.) The magnitudes of these modes oscillated with y in the inviscid region of the shock layer. This behavior is possible only because the shock layer has a finite thickness. They are also unlike Mack's higher modes (except for the second) in that the disturbance-pressure phase for all of these supersonic modes changed most across the inviscid region of the shock layer. (The disturbance-pressure phase change for Mack's higher modes occurs across the viscous region of the flow, i.e. the boundary layer.) In fact, the disturbance-pressure phase change for all of these supersonic modes through the boundary layer is comparable to that of Mack's second mode.

Another effect of the chemical reactions is to increase the size of the region of relative supersonic flow primarily by reducing the temperature in the boundary layer through endothermic reactions, increasing the density, and hence decreasing the speed of sound. This reduces the frequency of the higher modes; in particular, the most unstable one, the second mode. The higher modes in the reacting-gas cases are also more unstable relative to the corresponding perfect-gas modes. The first modes are, however, more stable.

Finally, the finite thickness of the shock layer has a significant effect on the first-mode solutions of all of the families. The effect on higher-mode, higher-frequency solutions does not seem to be as large as long as they are subsonic. This is perhaps what one would intuitively expect because the shock is likely "stiff" and hence difficult to perturb with smaller-wavelength, larger-wavenumber, higher-frequency disturbances. However, the nonparallel effects are known to be large for first-mode solutions, and so a complete quantitative description of the effects of the finite shock-layer thickness awaits either a PSE solution or a DNS analysis.

The inclusion of the bow shock is especially critical to studies of leading-edge receptivity as demonstrated by Zhong (1997). His DNS results over a blunt wedge show that the instability waves developed behind the bow shock consist of both first and second modes. His results also indicate that external disturbances, especially entropy and vorticity disturbances, enter the boundary layer to generate instability waves mainly in the leading-edge region.

3.1.5 Nonlocal Effects

It is now recognized that the growth rate of two-dimensional waves is only weakly affected by nonparallel effects. This was demonstrated for the Blasius flow by the computations of Gaster (1974) who used the method of multiple scales. This result was confirmed by PSE and DNS computations. PSE results were published by Bertolotti (1991) and by Chang et al. (1991) for supersonic Mach numbers. A good agreement was achieved with the multiple scale analysis of El-Hady (1991) at $M_e = 1.6$.

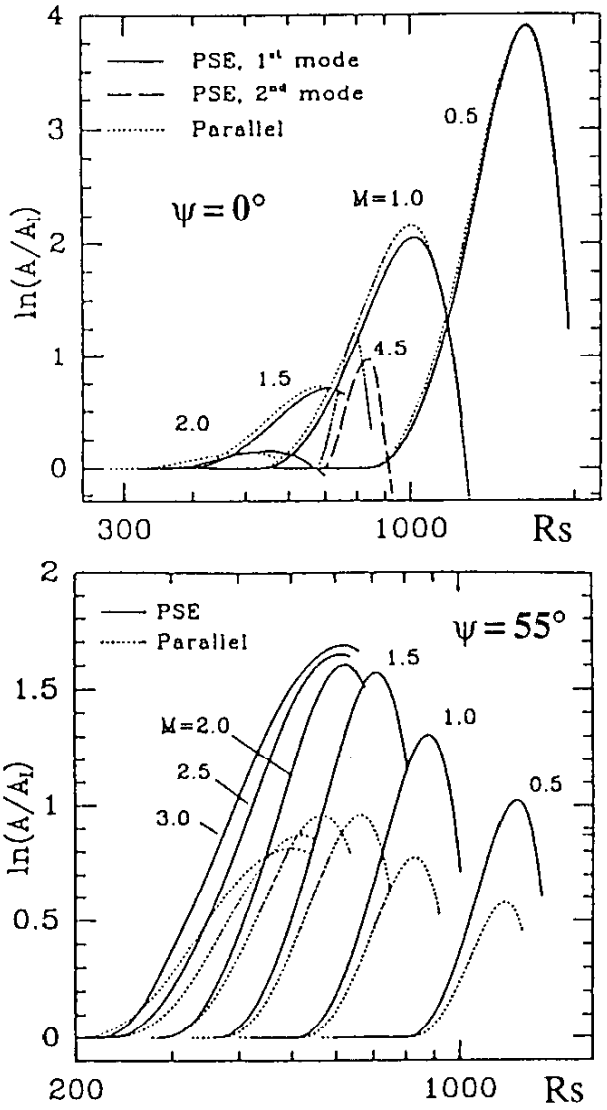

Figure 8. Integrated amplification rates for 2D waves, $\psi = 0°$, and oblique waves, $\psi = 55°$.

Figure 8 shows the integrated growth rates for a two-dimensional wave (the dimensionless frequency $F = 2\pi f \nu_e / U_e^2$ is 5×10^{-5}) at several Mach numbers. The streamwise Reynolds number R_x is defined as the square root of $\rho_e U_e x/(\mu_e M_e)$. The curves obtained under the parallel flow assumption are compared with the PSE results of Bertolotti (1991) with the growth rate computed at the maximum of the mass flux. The nonparallel effects become appreciable at $M_e = 4.5$ only.

This conclusion, however, is no longer valid for oblique waves, as it can be seen in Fig. 8 (Bertolotti 1991) which displays the evolution of the total growth rate for the same frequency, but with $\psi = 55°$. The mean flow nonparallelism exerts a strong destabilizing effect, and this effect increases with increasing Mach number. The importance of this difference on the *N-factor* could be significant for supersonic flows since the oblique waves are the most unstable ones and for hypersonic Mach numbers when first mode disturbances are dominant.

A detailed study of the nonparallel effects using PSE was also performed by Chang and Malik (1993). Trends qualitatively similar with those described before were reported for Mach 1.6 and 4.5 flat-plate flows. In general, nonparallel effects appear to be less significant for oblique waves near the lower branch of the neutral curve but become more important at higher Reynolds numbers near the upper branch.

3.2 Crossflow Instability

In the leading-edge region of a swept wing, both the surface and flow streamlines are highly curved. The combination of pressure gradient and sweep deflects the inviscid streamlines inboard. Because of the lower momentum fluid near the wall, this deflection is made larger within the boundary layer and causes *crossflow*, i.e. the development of a velocity component within the boundary layer that is perpendicular to the local edge-velocity vector. This crossflow profile exhibits an inflection point causing an instability in the form of crossflow waves. Reed and Saric (1989) give a review of the instabilities associated with this flow.

3.2.1 Transition correlation methods

The apparent complexity of the crossflow problem a few decades ago drove analysts to desperate measures in order to correlate transition. Owen and Randall (1952) introduced a *crossflow Reynolds number* $R_{cf} = W_{max}\delta_{10}/\nu_e$ (based on the maximum crossflow velocity and the boundary-layer height where the crossflow velocity is 10% of the maximum) as the governing parameter for crossflow-dominated transition. It was suggested that transition occurs when the crossflow Reynolds number becomes equal to about 150; a value for W_{max} of order 3% of the local inviscid speed is typical for wind-tunnel and flight tests (Poll 1984 discusses the details of this correlation). Pfenninger (1977) used the crossflow Reynolds number and a *crossflow shape factor* $H_{cf} = y_{max}/\delta_{10}$ in the design of supercritical airfoils. Dagenhart (1981) then considered stationary crossflow vortices and, instead of solv-

ing the linear stability equations each time, he used a table lookup of growth rates based on the profile characteristics: crossflow shape factor and crossflow Reynolds number.

In supersonic flow, Chapman (1961) and Pate (1978) made similar conclusions that crossflow Reynolds number correlates well with transition location. On a yawed cone, King (1991) found that there was no correlation with the traditional cross-flow Reynolds number. However, when he reformulated this parameter to include both compressibility and yawed-cone geometry effects, he found a correlation for both his and Stetson's (1982) data, but only as a function of azimuthal angle around the cone. Therefore, because this parameter depends on cone yaw angle, cone half-angle, and azimuthal angle, it is limited in its applicability to general geometries.

Reed and Haynes (1994) account for compressibility and cooling by introducing the *Howarth-Illingsworth-Stewartson* transformation (Howarth 1948; Illingsworth 1948, Stewartson 1949). They develop a new crossflow Reynolds number that correlates a rather wide range of data. The details are left to the original paper and the results are shown in Fig. 9.

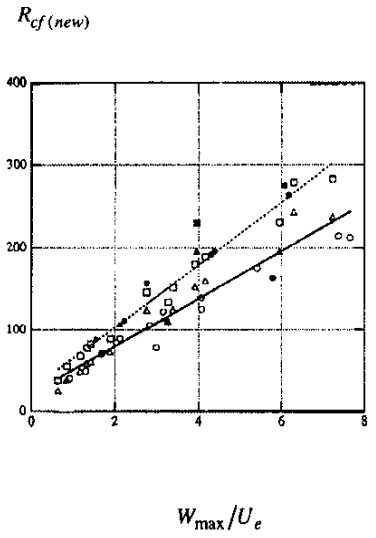

Figure 9. New crossflow Reynolds number (including compressibility and wall temperature) vs maximum crossflow velocity (solid line – noisy data; dashed line – quiet data) compared with experiments: King (1991) quiet □■;King noisy Δ▲;Stetson (1982) ○●;Holden et al. (1995) ●

The results of Fig. 9 are calculated using only basic-state profiles. Although the results of Fig. 9 are very encouraging, Reed and Haynes caution that this sort of correlation should only be used in *conceptual* transition prediction, design, and the evaluation of parameter trends. Once an airfoil shape is selected, nonlinear parabolized stability calculations are strongly urged. The present authors echo these comments.

3.2.2 The e^N Method in Three-Dimensional Flows

Strategies of integration. The extension of the e^N method to three-dimensional flows is not straightforward. The first reason is that the assumption $\beta_i = 0$ is not necessarily correct. Hence β_i must be assigned or computed. Several solutions have been proposed to solve this problem, see review in Arnal (1994). For instance, it is possible to use the wave packet theory and to impose the ratio $\partial\alpha/\partial\beta$ to be real. A simpler solution is to assume that the growth direction is the group velocity direction or the potential flow direction. In the case of delta wings, it can be assumed that there is no amplification in the spanwise direction.

After one of the previous assumptions for β_i has been adopted, one has to integrate the local growth rates in order to compute the *N-factor*. Several strategies are available:

- Envelope method: this strategy was previously described for two-dimensional, compressible flows.
- Fixed frequency/fixed spanwise wavenumber method: also used for first mode disturbances in two-dimensional, compressible flows.
- Fixed frequency/fixed wavelength method and fixed frequency/ fixed direction method: as a wave of fixed frequency moves downstream, the wavelength or the propagation direction of the disturbances are kept constant. These strategies resemble the previous one in this sense that the represents the envelope of several envelope curves.
- Streamwise *N-factors*/crossflow *N-factors*: the principle is to compute an *N-factor* for streamwise disturbances and another *N-factor* for crossflow disturbances. Transition is assumed to occur for particular combinations of these parameters.

As it can be expected, each strategy gives a different value of the *N-factor* at the onset of transition.

Examples of Application. Up to now there are only a few results dealing with the application of the e^N method for three-dimensional supersonic and hypersonic flows. The geometries which have been studied in these investigations are cones at angle of attack, swept (or delta) wings or rotating bodies without angle of attack.

Transition on a cone at incidence usually occurs earlier on the leeward line of symmetry than on the windward line. As there is no azimuthal mean velocity component along these lines, their stability properties are those of two-dimensional flows (at least in the framework of the classical stability theory).

Away from the windward and leeward rays, crossflow instability can dominate and cause transition.

Malik and Balakumar (1992) studied the linear stability of the three-dimensional flow field on a 5° half-angle cone at 2° incidence, for freestream conditions corresponding to those of King's experiments (King 1991) ($M_\infty = 3.5$, unit Reynolds number = 2.5×10^6/ft). As an example of result, Fig. 10 shows a comparison between measured and predicted transition fronts. The *N-factor* trajectories are plotted in the $x-\theta$ plane (θ is the azimuthal angle, which is 0° for the windward ray), with each line ending at $N = 10$. Along each line, the frequency is held constant, and the *N-factor* integration is carried out along the inviscid streamlines. The agreement is satisfactory, even if the predicted transition location is underestimated in the windward ray region. Early transition on the leeward ray is caused by the fact that the mean flow profiles are highly inflectional.

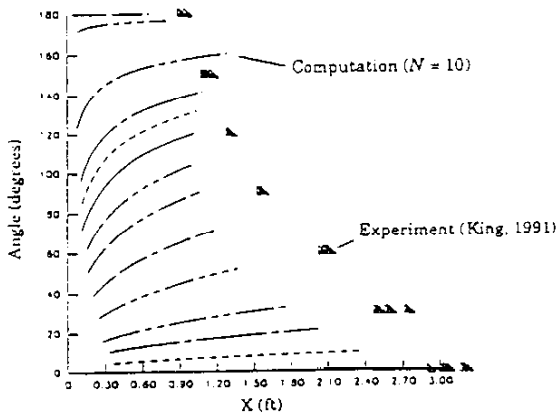

Figure 10. Comparison of experimental transition data with the computed (N = 10) location of transition

The problem becomes more complicated at higher Mach numbers due to the appearance of second-mode disturbances. In the framework of the ESA TRP mentioned before (paragraph 3.1.2 experiments and computations (local theory) have been performed for a cone at Mach 7 and 2° angle of attack (Tran et al. 1995) (Arnal et al. 1996). Figure 11 shows the integrated growth rates of first and second-mode disturbances at the measured transition locations on the leeward ray (denoted as L in the figure) and on the windward ray (denoted as W). Results at zero angle of attack are given for comparison. The most striking feature is that N increases from windward to leeward ray for first mode disturbances, whereas it decreases for second-mode disturbances. As a consequence, predicted transition occurs earlier on the leeward ray than on the windward ray (in agreement with the experiments) if one assumes that it is triggered by first mode disturbances. But transition would appear earlier on the windward ray if it were induced by second-mode disturbances. This could be an indication that second-mode, high frequency disturbances do not play any major role in these experiments, even if their *N-factors* are much larger than those of first mode disturbances.

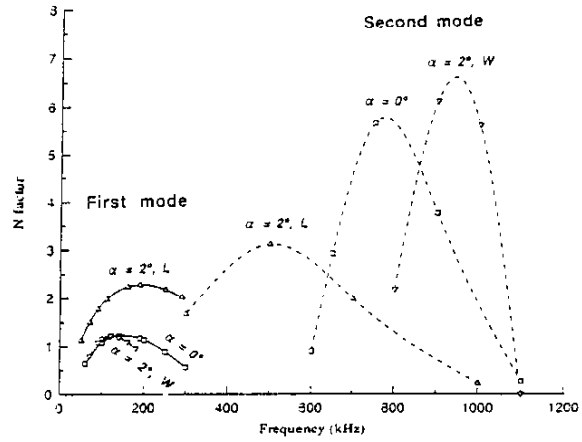

Figure 11. *N-factors* at transition on a cone at angle of attack (windward and leeward rays)

The stability characteristics along the leeward and windward rays of a cone at incidence were investigated by Hanifi (1995) using PSE approach (NOLOT code, developed at FFA/KTH in Sweden and DLR in Germany Hanifi et al. 1994). The computations were performed for conditions corresponding to King's experiments (King 1991) and to Krogmann's experiments Krogmann 1977). Due to the rather low values of M_∞ (3.5 and 5), only first mode disturbances were present. The movement of transition as a function of angle of attack was fairly well predicted by the e^N method. It was also observed that the nonlocal effects were larger on the windward meridian than on the leeward meridian.

Transition on a swept wing leading edge model at Mach~3.5 was investigated by Cattafesta et al. (1995). Numerical results obtained with the e^N method (local theory, envelope strategy) were compared to experimental transition location measured in the NASA Langley "quiet tunnel". It was found that traveling disturbances with $N \cong 13$ provided a good correlation with experiments over a range of unit Reynolds numbers and angles of attack.

The transition process on a delta wing was investigated at Imperial College gun tunnel within ESA TRP Tran et al. (1995). A large number of parameters (angle of attack, angle of sweep, unit Reynolds number, leading edge bluntness) was investigated. Linear, local stability computations have then been performed for a few experimental configurations (Arnal et al. 1996). With sharp leading edges, the boundary layer development was nearly two-dimensional, and experimental

transition locations were correlated with *N-factors* between 1 and 2. As soon as the leading edge radius was increased, the boundary layer flow became highly three-dimensional, and transition was induced by crossflow instability at much larger values of the *N-factor*. From this (rather limited) series of computations, it appears that the *N-factors* at transition are likely to be very different depending on the type of dominant instability. Reed and Haynes Reed and Haynes (1994) investigated the local instability properties of a supersonic rotating cone at zero angle of attack, which was used as a model of a swept wing. The results were then used to develop a simple criterion which was applied to several experiments on cones at angle of attack.

Shortcomings of the *N-factor* Method. As the e^N method is based on linear stability only, receptivity and nonlinear mechanisms are not taken into account. In addition the nonparallel effects are neglected in the local procedure, and it has been shown that they could be important for oblique waves.

Several particular problems arise for three-dimensional flows. The first one is to choose the "best" strategy of integration of the *N-factor*. The envelope method is widely used, but its physical meaning is not clear in many cases. A classical problem occurs for swept wings, especially in transonic conditions: in the vicinity of the point of minimum pressure, rapid variations in φ_M can be observed when the dominant instability suddenly changes from the crossflow to the streamwise type. The other strategies are often used in order to avoid these discontinuous (and probably unphysical) evolutions. In particular, this problem does not appear with PSE computations.

From a practical point of view, the most important issue is the value of the *N-factor* at the onset of transition. Concerning two-dimensional flows, it is has been shown (paragraph 3.1.2) that the e^N method with $N \cong 10$ can be applied to predict transition for a wide range of flows in a low background turbulence environment. In three-dimensional flows, the results depend, of course, on the strategy which is chosen to compute the *N-factor*, but, even with the same strategy, the results are not very clear. In fact, all the strategies produce a large scatter in the values of N at the onset of transition. A possible reason is that crossflow and streamwise instabilities are not initiated by the same type of forced disturbances. For instance, the crossflow disturbances are very sensitive to micron-sized roughness elements which have no effect on streamwise disturbances, see Radeztsky et al. (1993). Another reason is that there exists a multiplicity of nonlinear processes before the breakdown to turbulence, depending on the relative part of stationary and travelling unstable modes. In particular, it is now clear that the extent of the nonlinear regime is much larger for three-dimensional flows than for two-dimensional flows, resulting in a larger scatter in the (linear) *N-factor* at transition.

In spite of these deficiencies, the e^N method can help to understand the physics of the transition phenomena. As for two-dimensional flows, it is useful for parametric studies, as soon as the *N-factor* for the different types of disturbances has been fixed from some reference case.

3.3 Görtler Instability

Boundary layers over concave surfaces are subject to a centrifugal instability that appears in the form of stationary streamwise-oriented, counter-rotating vortices usually called Görtler vortices. A description of the physical mechanisms and a recent review is given by Saric (1994b).

A graphic example of this mechanism can be observed as streamwise surface striations on reentry vehicle heat shields. The differential ablation between the nose cone and the heat shield of reentry vehicles produces a concave surface which induces a Görtler instability. The vortices then cause spanwise variations in the heat transfer.

3.3.1 Swept-Wing Flows and Stagnation Flows

Hall (1985) has shown that beyond a very small sweep angle, the principal instability on a swept wing with concave curvature is a crossflow instability and not a Görtler instability. This analysis reduces the concern about Görtler problems in swept-wing flows. Bassom and Hall (1991) extend these ideas to the receptivity question.

Another issue that frequently comes up in the context of Görtler vortices concerns stagnation flows. The Rayleigh circulation criterion appears to be satisfied near the stagnation region of bluff bodies and a Görtler instability has been a suspect regarding the origin of streamwise vorticity in a boundary layer such as observed by Klebanoff et al. (1962). Stuart (1984) has shown conclusively that an instability does not exist.

3.3.2 Compressibility Effects

A recent application for information regarding transition induced by Görtler vortices in a compressible flow is in the design of "quiet" supersonic wind tunnels. The major source of freestream noise is radiation from the turbulent boundary layers on the nozzle. Since the accelerating pressure gradient generally stabilizes Tollmien-Schlichting instabilities, transition is induced by Görtler vortices on the concave region of the nozzle (Beckwith et al. 1985, Chen et al. 1985). Efforts to calculate the growth of the instability with compressibility are given by Hämmerlin (1961), Kobayashi and Kohama (1977), El-Hady and Verma (1983a,b), Tumin and Chernov (1988),

and Jallade et al. (1990) using the separation-of-variables technique without the large spanwise wavenumber limit. Hall and Malik (1989) analyze the role of compressibility within the large wavenumber limit. As mentioned earlier, these results will have limited applicability. Recently Dando and Seddougui (1991) and Dando (1992) completed analyses for two-dimensional and three-dimensional boundary layers, respectively in the large Görtler number limit (inviscid flow). Both papers use unit Prandtl number and Chapman viscosity law approximations that have been shown to be grossly incorrect for other types of instabilities in high-speed flows. In the absence of an experiment, there is no telling whether these approximations are valid for Görtler vortices.

Spall and Malik (1989) integrate the linearized parabolic stability equations and show that compressibility is stabilizing but the stabilization is reduced as hypersonic speeds are approached. Hall and Fu (1989) and Fu et al. (1993) assess the role of Sutherland's viscosity law and real-gas effects on the linear stability of Görtler vortices and remove the restrictions of previous analyses. Fu and Hall (1991a, 1991b) then extend this work to nonlinear effects and secondary instabilities. Fu and Hall (1994) demonstrate how crossflow affects Görtler instabilities. These last five papers by Hall and his group have jumped so far ahead of the experimental capability and present knowledge base that it is difficult to assess their value. We know that some of the approximations made on the mean flow might not be appropriate for streamwise traveling instabilities. On the other hand, this body of work may offer some insight into operative mechanisms that a well-established experiment could examine. The initial experimental work by de Luca et al. (1993) is a step in the right direction.

3.4 Attachment-Line Problems

It is not easy to give an accurate definition of the attachment line of a three-dimensional body, except for simple geometries such as symmetrical bodies of constant chord and infinite span: it is the line along which the static pressure is maximum. More intuitively, the attachment line represents a particular streamline which separates the flow into one branch following the upper surface and one branch following the lower surface.

Let us consider the simplest case of a swept cylinder of constant radius R. In the coordinate system (X,Z,y) linked to the cylinder, Z coincides with the attachment line, X is normal to Z on the cylinder surface, and the y axis is normal to the wall. U and W are the projections of the mean velocity along X and Z. U_e depends linearly on $X\,(U_e = kX)$. If the infinite span assumption is used, W_e is constant. The Reynolds number $\overline{R}$ and the reference length μ are defined as:

$$\overline{R} = \frac{W_e \eta}{\nu_e} \text{ and } \eta = (\nu_e/k)^{1/2} \qquad (11)$$

For low-speed flows, η is close to the displacement thickness δ_1. For high-speed flows, Poll (1985) introduced a modified length scale η^* and a modified Reynolds number, $\overline{R}^*$ which have the same definitions as η and $\overline{R}$, except that ν_e is replaced by ν^*. The latter quantity is the kinematic viscosity computed at a reference temperature T^* which may be estimated from the following empirical relationship (Poll 1985):

$$T^* = T_e\left[1 + 0.1(T_w/T_e - 1) + 0.6(T_{aw}/t_E - 1)\right] \qquad (12)$$

T_w and T_{aw} denote the wall temperature and the adiabatic wall temperature, respectively.

The equations for a yawed infinite cylinder are obtained from the 3D boundary-layer equations by imposing that all spanwise derivatives are identically zero. If the flow is laminar, self-similar equations can be obtained by using appropriate transformations. When the freestream Mach number is zero, solutions of these equations are also solutions of the exact Navier-Stokes equations. Solutions for compressible flows have been published, e.g. Reshotko and Beckwith (1958) who used Stewartson's transformation. It is also possible to introduce Levy-Lees variables, which lead to a system of ordinary differential equations with three parameters: the Mach number M_e, the temperature ratio T_w/T_{aw} and a suction parameter K. M_e is the spanwise Mach number based on the velocity and on the temperature at the boundary-layer edge. Only the case $K = 0$ will be considered in this section.

Most of the transition problems which have been discussed so far take place some distance downstream of the attachment line. However, transition phenomena which are likely to occur along this streamline exhibit some peculiar features which will be summarized in this section. Distinction will be made between "natural" transition mechanisms (transition occurs through the selective amplification of boundary layer eigenmodes), leading-edge contamination (transition occurs through a "bypass" process induced by a source of large disturbances such as end plates parallel to the freestream) and boundary-layer tripping by roughness elements. In the latter case, distinction will be made between roughness elements on and slightly off the attachment line.

3.4.1 "Natural" Transition on Attachment Line

Linear Stability Theories for Incompressible Flows. The simplest idea is to introduce small traveling disturbances similar to TS waves:

$$(u', v', w', p') = (u, v, w, p)\exp(\alpha Z)\exp[i(\alpha Z - \omega t)] \qquad (13)$$

The parallel-flow approximation is then used. With the condition $U = 0$, the fourth-order differential equation is exactly the Orr-Sommerfeld equation written for the attachment-line profile $\overline{W}$.

It is possible to follow a more rigorous approach by considering a special class of small-amplitude disturbances, first introduced by Görtler (1955) and Hämmerlin (1955). These Görtler-Hämmerlin (GH) disturbances are of the form:

$$u' \sim xu\exp(\sigma Z)\exp[i(\alpha Z - \omega t)] \qquad (14)$$

$$v', w', p' \sim (v, w, p)\exp(\sigma Z)\exp[i(\alpha Z - \omega t)] \qquad (15)$$

As for the TS waves, u, v, w and p depend only on y. There is no real justification for the X-dependence of the u' fluctuation. Görtler chose it for reasons of "mathematical feasibility", but recent computations performed by Spalart (1988) supported this assumption.

Introducing (14) and (15) into the Navier-Stokes equations and linearizing in u, v, w create, of course, an eigenvalue problem. But, in contrast to the Orr-Sommerfeld approach (TS waves), the system of ordinary differential equations are obtained without using the parallel-flow approximation. In other words, the GH disturbances are exact solutions of the linearized Navier-Stokes equations. This system is sixth order, while the Orr-Sommerfeld equation is fourth order.

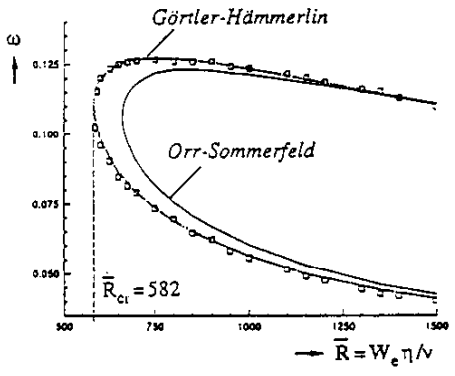

Figure 12. Neutral curves computed for TS disturbances and for GH disturbances. Symbols: Hall, Malik and Poll. Lines: ONERA/CERT

Figure 12 presents a comparison between the neutral curves computed for the TS-type disturbances (Orr-Sommerfeld equation) and for the GH disturbances. Two series of computations are presented for the GH disturbances: the first one was published by Hall et al. (1984), the second one was obtained at ONERA/CERT by Arnal (1993) with a completely different numerical technique. The critical Reynolds numbers $\overline{R}_{cr}$ are 662 and 582 for the TS and for the GH disturbances, respectively. In the unstable region, the growth rates of the latter are significantly larger than those of the former. Pfenninger and Bacon (1969) and Poll (1978) observed naturally occurring disturbances along the attachment line of different swept models at low speed. It was found that such disturbances existed above a critical value of R_θ close to 230, in excellent agreement with the linear stability results for the GH disturbances.

Assuming that the mean flow is uniform in the spanwise direction, application of the e^N method along the attachment line is straigthforward. For a given frequency, σ is constant in the Z-direction, and the transition location Z_T is given by:

$$Z_T = \frac{N}{\sigma_{\max}} \qquad (16)$$

with $Z = 0$ corresponding to the origin of the attachment line. $\sigma_{\max}$ denotes the value of σ computed for the most unstable disturbances. Values of N around 10 correlate the available experimental data at low speed (Arnal 1993).

The important result is that "natural" transition on the attachment line will appear as soon as $\overline{R}$ exceeds the critical Reynolds number $\overline{R}_{cr}$ deduced from the linear theory. For $\overline{R} > \overline{R}_{cr}$, the value of $\overline{R}$ determines the value of $\sigma_{\max}$ and then the transition location Z_T.

Extension to Compressible Flows. Unfortunately, it is not possible to use the GH approach for oblique waves, because the stability problem becomes ill posed. This implies that this approach cannot be used for attachment-line problems at high speed, because oblique waves become dominant as soon as M_e exceeds a value close to 1. If one wants to follow a classical, linear stability approach, the only possibility is to consider TS-type disturbances having a chordwise wavenumber component; i.e. equation (13) is replaced by:

$$u' \sim Xu\exp(\sigma Z)\exp[i(\alpha Z + \beta X - \omega t)] \qquad (17)$$

The stability problem is then reduced to the usual 2D stability problem on a flat plate, the three-dimensionality of the basic flow being taken into account by the particular shape of the attachment line mean velocity profile. Of course, there is no evidence that TS-type waves would be the most unstable disturbances along a compressible attachment-line flow.

Linear stability results based on the TS-type approach have been published, for instance, by Malik and Beckwith (1988), Arnal et al. (1991) and Da Costa (1990). The computations by Malik and Beckwith were performed for flow conditions corresponding to the experiments of Creel et al (1987) in the "quiet tunnel" at NASA Langley ($M_\infty = 3.5$, $M_e = 2.39$). It was found that the most unstable waves propagate with a

wavenumber angle φ close to 50-60°. For an adiabatic wall, the critical Reynolds number is $\overline{R}_{cr} = 640$, or $\overline{R}^*_{cr} = 391$. As for flat-plate flows, cooling the wall has a strong stabilizing effect. Similar results were obtained by Arnal et al. (1991). Da Costa (1990) performed computations related to his experiments on a swept cylinder $(M_\infty = 7.1, M_e = 5.13)$. The critical Reynolds number for adiabatic conditions is $\overline{R}_{cr} \cong 172$. This surprising result means that "natural" transition is likely to occur at a Reynolds number which is smaller than that corresponding to leading-edge contamination ($\overline{R}^*_{cr} \cong 250$ see next paragraph). For a wall temperature ratio T_w/T_{aw} around 0.4, $\overline{R}_{cr}$ increases up to 13~500, i.e. $\overline{R}^*_{cr} \cong 4500$.

Simple Criteria for "Natural" Transition. Bushnell and Huffman (1967) observed that laminar flow on a smooth attachment line could exist up to at least $R_{\infty,D} = 8\times10^5$, where $R_{\infty,D}$ is the Reynolds number based on freestream conditions and leading-edge diameter. This criterion is valid for Mach numbers M_∞ between 2 and 8, and for sweep angles larger than 40°. Another criterion proposed by Poll is $\overline{R}^* \cong 660$ at transition. It will be discussed later on.

Experimental Results. There are only a few experimental results available for the problem of "natural" transition along the attachment line of swept models at high-speed conditions. Careful experiments were conducted by Creel et al. (1987) in the "quiet tunnel" at NASA Langley; under adiabatic conditions, transition was found to occur for $\overline{R}$ close to 700, a value which is nearly twice the theoretical value computed by Malik and Beckwith (1988). However, it is interesting to note that the experimental value is close to that of the critical Reynolds number $\overline{R}$ computed for incompressible flow. This observation led Poll to the conclusion that $\overline{R}^* \cong 660$ could be a "universal" value for transition on smooth leading edges. The most interesting finding of Creel's experiments is that the wind tunnel noise has no effect on the "natural" transition Reynolds number (see Fig. 16). This can be explained by a theory on the receptivity of supersonic laminar boundary layer to acoustic disturbances; calculations by Gaponov demonstrated that external noise cannot generate unstable waves when the boundary-layer thickness is constant, as it is the case along the attachment line.

The measurements by Gaillard (1993), shown in Fig. 13, have been performed on circular cylinders as well as on cylinders having a nearly flat surface around the attachment line (in order to reach large values of $\overline{R}^*$). The experimental results for $T_w/T_{aw} \cong 0.4$ are plotted in Fig. 13. It can be seen that the transition Reynolds number decreases when the spanwise Mach number increases. Gaillard also studied the influence of the wall temperature. He found that cooling has a small stabilizing effect for spanwise Mach numbers up to about 5, and then a small destabilizing effects for larger values of M_e. All of these results completely disagree with the trends predicted by the linear stability theory when considering TS-type disturbances.

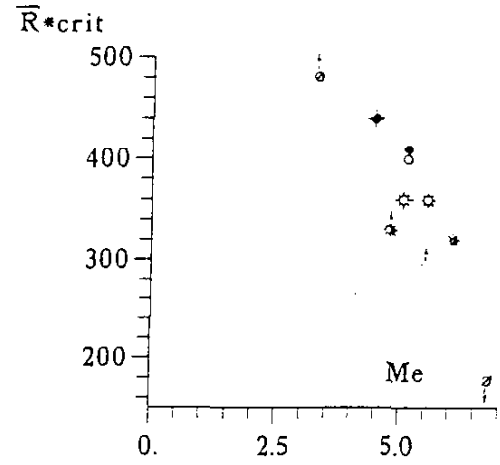

Figure 13. Transition Reynolds numbers as a function of M_e on a smooth leading edge without end plates $(T_w/R_{aw} \cong 0.4)$ From (Galliard 1993).

Recent experiments were performed by Holden et al. (1994) in the Calspan 48-inch shock tunnel on a highly swept cylinder, at freestream Mach numbers from 10 to 12. Attachment line measurements with a smooth leading edge, with end plates and with roughness strips were reported. With a smooth leading edge, transition was observed for values of $\overline{R}^*$ from 600 to 800. The corresponding freestream Reynolds numbers based on cylinder diameter were above 8×10^5. However, turbulent bursts were observed at $\overline{R}^* \cong 550$, which could be attributed to a misalignment of the nosetip with the freestream.

Experiments were conducted by Murakami et al. (1995), in the hypersonic Ludwieg-tube wind tunnel of DLR at Mach numbers $M_\infty = 5$ and 6.9 (spanwise Mach numbers $M_e = 1.9$ and 2.9). Transition was detected on swept cylinders by liquid-crystal technique. In the absence of gross disturbance sources, the Reynolds numbers $\overline{R}^*$ for "natural" transition were in the range 680-750, corresponding to values of $R_{\infty,D}$ in the range $0.9\text{-}1.2\times10^6$. These values agree with Creel's data.

3.4.2 Attachment-Line Contamination by End Plates

Empirical Criteria. Leading edge contamination is likely to occur when a swept body is attached to a solid surface (fuselage, wind-tunnel wall, etc.). This problem has been widely studied for low-speed flows (see reviews in Poll 1978 and Arnal 1992 for instance), and a simple criterion, based on the value of $\overline{R}$, was developed by Pfenninger (1965). If $\overline{R}$ is lower than 250, the bursts of turbulence convected along the

wall are damped and vanish as they travel along the attachment line. However, for $\overline{R} > 250$, these bursts are self-sustaining. They grow, overlap and the leading-edge region becomes turbulent.

Several series of experiments were devoted to the study of leading-edge contamination at high speeds. In most of the cases, end plates were used as sources of gross disturbances. The first attempt to quantify attachment-line contamination in these conditions is due to Bushnell and Huffman (1967), who observed that the boundary-layer flow on the leading edge became turbulent if $R_{\infty,D} > 2\times10^5$ (M_∞ between 2 and 8, sweep angle larger than 40°).

Poll (1985) analyzed available experimental data for $0 < M_e < 6$ and showed that leading-edge contamination occurs for $\overline{R}^* = 245 \pm 35$, as illustrated in Fig. 14. There are no effects of Mach number, unit Reynolds number and wall temperature.

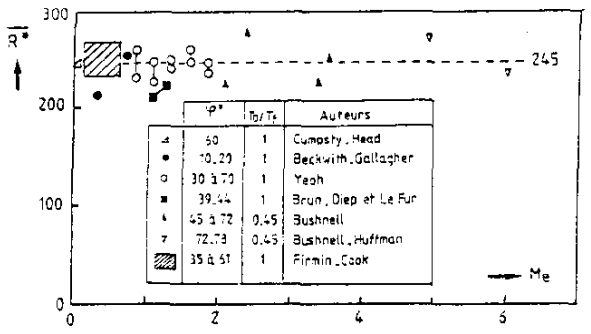

Figure 14. Leading edge contamination criterion at high speed. From (Poll 1985)

Experimental Results. In the experiments of Murakami et al. (1995), it was found that disturbances generated by end plates parallel to the incoming flow induced leading edge contamination at free stream Reynolds numbers $R_{\infty,D}$ of approximately 0.15 to 0.5×10^6, in reasonable agreement with Bushnell's criterion. When expressed in term of $\overline{R}^*$, leading-edge contamination occurred for values which are significantly larger than those due to Pfenninger's criterion and other experimental data (mean value around 300-350). The explanation could be that the disturbances generated at the end-plate/cylinder junction were small because the boundary layer on the end plate was laminar.

The influence of the end-plate length was investigated in detail by Costa (1990) and Gaillard (1993) at CEAT Poitiers. For "long" end plates (i.e. $L/D > 1$, where L is the plate length), leading-edge contamination was observed for $\overline{R}^* \cong 250$. For $L/D = 0.79$, the attachment-line boundary layer became turbulent for $\overline{R}^* \cong 330$. This result is in agreement with the findings of Murakami et al. (1995) and supports their explanation for the increase of $\overline{R}_c^*$ in the case of "short" end plates. A more surprising observation was made in the case of a "very short" end plate $(L/D = 0.53)$; in this case, the Reynolds number at attachment-line contamination was reduced to about 200. The explanation proposed by Gaillard is that, for "long" and "short" end plates, the main source of gross disturbances is the boundary layer (either turbulent or laminar) at the end plate/cylinder junction. For "very short" end plates, the shock generated at the plate leading edge begins to play the dominant role, leading to a decrease in $\overline{R}_c^*$.

3.4.3 Boundary-Layer Tripping with Roughness Elements on the Attachment Line

Low Speed Flows. As far as low-speed flows are concerned, a detailed experimental study was carried out by Poll (1978), who investigated the response of the attachment line boundary layer to the presence of wires, the axis of which was normal to the leading edge direction. If the wire diameter, d, is made dimensionless with the length scale η defined previously, four d/η ranges have to be distinguished, as it is illustrated in Fig. 15:

- Region I: for $0 < d/\eta < 0.7$, the wire has no effect, and transition is triggered by linear mechanisms; the main parameter is the freestream disturbance level.
- Region II: for $0.7 < d/\eta < 1.5$, the wire begins to control transition. The location of the first turbulent spots moves closer to the wire when $\overline{R}$ is increased.
- Region III: for $1.5 < d/\eta < 1.9$, the flow is either fully turbulent or fully laminar behind the wire. At a fixed value of d/η this change in the boundary layer structure occurs for a very small variation of $\overline{R}$. Gaster (1967) and Cumpsty and Head (1967) observed this phenomenon which Poll called "flashing".
- Region IV: for $d/\eta > 1.9$, turbulent bursts always appear immediately behind the wire. But, if $\overline{R}$ is lower than about 250, they decay more or less rapidly as they are convected along the attachment line. If $\overline{R}$ is greater than this critical value, the size of the burst increases and leading-edge contamination occurs. It is clear that there is a strong similarity with the leading-edge contamination induced by a wing-wall junction. One can deduce that there exists a minimum Reynolds number $(\overline{R} \cong 250)$ beyond which every turbulent structure generated by a gross disturbance source becomes self-sustaining, develops and makes the leading edge turbulent.

boundary layer is disturbed locally by the roughness element.

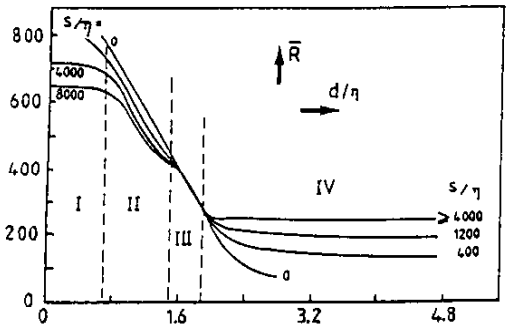

Figure 15. Location S where the first turbulent bursts are observed. S is measured from the wire along the attachment line. From (Poll 1978).

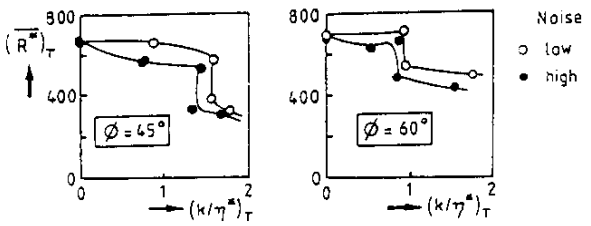

Figure 16. Transition Reynolds number along the attachment line with small roughness elements. From (Creel et al 1987).

High Speed Flow. Region I was studied by Creel et al. (1987) in the "quiet tunnel" at NASA-Langley (freestream Mach number $M_\infty = 3.5$). Transition was detected along the attachment line of a swept cylinder, without disturbance sources and with small roughness elements. By changing the operating conditions, the freestream noise levels were varied from very low values to much higher values approaching those in conventional wind tunnels. The main results are reported in Fig. 16, which shows the evolution of $\overline{R}^*$ at transition as function of k/η^* (k is the roughness height). The following effects are observed:

- On smooth cylinders, "natural" transition occurs for $\overline{R}^* = 650$ to 700, in agreement with the lower limit of Fig. 16 for $k = 0$. As stated previously (section 3.4.1), the acoustic disturbances generated by the boundary layers developing along the nozzle walls have no effect on the transition Reynolds number.
- Small trips have no well-defined influence on transition Reynolds number until a "critical value" of k/η^* is reached. This value is around 0.9 for $\phi = 60°$ and around 1.5 for $\phi = 45°$. As soon as this critical size is exceeded, $\overline{R}^*$ at transition decreases rapidly, but a detailed comparison with Fig. 16 is not easy. For fixed values of ϕ and k/η^*, an increase in the wind-tunnel noise decreases the transition Reynolds number. The interpretation by Creel et al. is that the external noise generates unstable disturbances at the location where the laminar

Boundary-layer transition data with trip wires were obtained at DLR by Murakami et al. (1995) and at CEAT by Da Costa (1990) and Gaillard (1993). Trends in the dependence of the $\overline{R}^*$ transition Reynolds number on the dimensionless roughness height were similar to those observed in other investigations, i.e. there exists a "critical" value of k/η^* for which transition Reynolds number stars to decrease when the trip diameter increases; in region II, the behavior of $\overline{R}^*$ at transition strongly depends on the spanwise Mach number.

Transition phenomena with roughness elements located on the attachment line of a swept cylinder were investigated at ITAM Novosibirsk by Skuratov and Fedorov (1991) at $M_\infty = 6$. The tripping devices were small steel elements of rectangular section. Runs were performed at fixed roughness height and different unit Reynolds number values. Values of $\overline{R}^*$ at "natural" transition (region I) have not been reported. When k/η^* increases, the transition Reynolds number in regions II and III exhibit a behavior which is qualitatively similar to that of Fig. 16. For large values of k/η^*, the region of self-sustaining turbulence (region IV) is observed at a constant Reynolds number $\overline{R}^*$ around 240. The same value was found to correlate data with sand roughness strips.

Boundary layer tripping experiments on swept cylinders have been carried out at ONERA at Mach 10 (Arnal et at. 1991). The tripping elements consisted of small steel cylinders (height = diameter) fixed on the attachment line with their axis normal to the wall. As the maximum value of $\overline{R}^*$ was

around 400, only little information was obtained in regions I, II and III. For k/η^* larger than 2, turbulent flow developed as soon as $\overline{R}_*$ exceeded a critical value of 250.

In the experiments performed by Holden et al. (1994) on a swept cylinder with roughness strips, two series of results have been reported. One corresponds to values of k/η^* between 0.8 and 2 (regions II and III); in this case, the transition Reynolds numbers were in satisfactory agreement with the correlation of Fig. 15. Other results were obtained for highly tripped configurations (k/η^* between 2 and 3), leading to transition Reynolds numbers $\overline{R}^*$ around 330, a value which is significantly larger than the usual limit $\overline{R}^*$ =250.

3.4.4 Boundary-Layer Tripping with Roughness Elements off the Attachment Line

The effect of roughness element chordwise location was studied at ONERA on a swept cylinder at Mach 10 (Arnal et al. 1991). The tripping devices (small cylinders as before) were placed at non-zero values of θ_k, where θ_k denotes the azimuthal angle of the roughness location, $\theta_k = 0°$ corresponding to the attachment line.

The results are summarized in Fig. 17 for two sweep angles. The full circles correspond to configurations for which the wall heat flux distribution was of the turbulent type downstream of the roughness element. The open circles correspond to configurations for which the roughness height was not sufficient to trigger transition. The circles with a cross refer to "intermediate cases": the wall heat flux distribution was neither laminar nor turbulent.

It is clear that the minimum roughness height which is necessary to trigger transition increases with θ_k. As previously stated by Morrisette (1976) and Poll (1985), the attachment line is the location where a laminar boundary layer is the most sensitive to roughness elements.

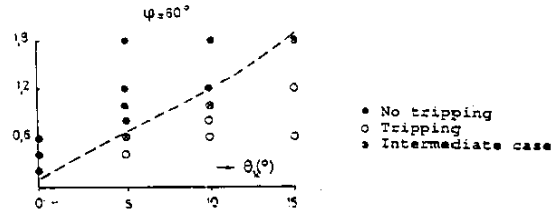

Figure 17. Effect of roughness location on boundary layer tripping. From (Arnal et al 1991).

3.4.5 Blunt-Body Problem

Using a multiple-scales analysis, Reshotko and Khan (1980) showed that for a blunted flat plate, upstream of the location where the boundary layer swallows the entropy layer (layer of air coming through the strong part of the bow shock wave), both the boundary layer and the shock layer can become unstable in a generalized inflectional sense. After the boundary layer swallows the entropy layer, the boundary-layer profiles asymptote to those for a sharp leading edge and their stability characteristics follow suit. Within the swallowing region, the stability characteristics are also affected by the fact that the shock-layer flow at the edge of the boundary layer is non-uniform in y. This seems to be stabilizing for the first mode but destabilizing for the second mode. Equivalent studies for blunted cones had been hampered by the unavailability of reliable laminar flowfield calculations particularly over the first 20 or so nose radii. Computational results by Malik (1988) for the blunted cone of the experiment of Stetson et al. (1984) $(M_\infty = 8, \theta_c = 7°)$ qualitatively resemble experimental features including presence of the second-mode frequency band. But, they significantly underestimate $Re_{\min,\mathrm{crit}}$ for both the sharp and blunted cones. For the sharp cone, this may be due to the very small bluntness of the experimental cone. For the blunted cone, the discrepancy may stem from an inadequate calculation of the basic flow in the vicinity of the nose. Malik et al. (1990) point out further that their computations did not detect the instability in the shock layer as observed by Stetson et al. (1984). No theory has offered explanation for the observed growth at a frequency band above the second mode but below the third. Stetson speculatively identified this feature as a nonlinearity, possibly a harmonic of the second mode.

In the light of these uncertainties, Herbert et al. (1992) concentrated on a correct calculation of the basic laminar flow over a blunted cone as prerequisite for the subsequent stability calculations. Since PNS methods are not reliable in the nose region, they use a Navier-Stokes method out to $s/R = 5$ and a PNS method downstream of that location. Care is also given to the accuracy of the derivatives of the flow profiles since stability calculations are sensitive to these derivatives. Early stability calculations showed good agreement with Malik et al. (1990) but were only qualitatively reminiscent of the Stetson et al. (1984) data. Not addressed by Malik et al. (1990) or Herbert et al. (1992) is the relationship between the stability characteristics to features of the swallowing phenomenon. A recent work by Johnson et al. (1997) obtains the flowfield over a spherically blunted cone-like body using a Navier Stokes method. They showed the existence of a generalized inflection point in the shock layer outside the boundary layer that progressed from midway in the shock layer at $s/R = 2$ to near the outer edge of the boundary layer at $s/R \approx 7$. Their stability calculations for their assumed flight conditions however found no growing disturbances in this portion of the

flowfield. Clearly, the effects of nose blunting on stability and transition are not resolved.

3.5 Receptivity and roughness

3.5.1 Use of Ground Based Facilities

Transition experiments done into the 1960's and the transition Reynolds number correlations developed from them included among the factors affecting transition a so-called "unit Reynolds number effect," which usually showed itself as an increase in transition Reynolds number with increase in wind-tunnel total pressure. Reshotko (1969) pointed out that this is in fact due to the spectral character of the disturbance environment. To that point, the disturbance environment had not been specifically considered among the experimental factors affecting transition. Morkovin (1969) enlarged upon this by pointing out that one must determine the means by which the disturbance environment generates growing disturbances in a boundary layer, a process that he called "receptivity." Also in this time frame, Pate and Schueler (1969) showed convincingly that transition behavior in conventional supersonic tunnels was dominated by the sound radiated onto wind-tunnel models by the turbulent boundary layers on the tunnel walls - an artifact of wind-tunnel testing with no flight counterpart. This was confirmed by the important flight experiments of Dougherty and Fisher (1980). Their transition cone had already been run in many transonic and supersonic wind tunnels throughout the world. In wind tunnels for $M > 2$ they consistently obtained the familiar transition "bucket" with a Re_{tr} minimum between Mach numbers 4 and 5. However, in flight experiments with the cone model mounted ahead of the fuselage of an F-15 aircraft, the transition Reynolds number corrected to adiabatic wall conditions showed consistent increase with Mach number over the entire flight speed range whereas the values for Re_{tr} obtained in conventional wind tunnels started falling at $M > 1.6$.

The Pate and Schueler (1969) work led directly to the development of "quiet" supersonic wind tunnels. A "conventional" quiet supersonic tunnel is one where laminar boundary layers are maintained over as much of the nozzle and test section walls as possible. The character, limitations and accomplishments of the NASA-Langley $M = 3.5$ pilot quiet tunnel are described by Beckwith et al. (1990). Quiet supersonic tunnels have been developed further and shown to give flight-quality transition data (Wilkinson 1997). At $M > 8$, even conventional tunnels with turbulent tunnel-wall boundary layers display an essentially quiet behavior as the primary instability frequency bands tend to be above the tunnel noise spectrum. However if the path to transition involves subharmonic frequencies, then those tunnels may not be sufficiently quiet. Conventional supersonic and hypersonic tunnels may still be used to study TS, swept attachment-line and crossflow instability and transition provided that it is ascertained that the results are not affected by tunnel noise. Reed et al. (1997) contain additional discussions on this topic.

3.5.2 What is Known About Supersonic Receptivity

The disturbance environment affecting boundary layers on vehicles in flight can come from two sources: a) atmospheric disturbances or particulate effects as modified by passage through the inevitable shock waves, and b) mechanical and acoustic disturbances coming from other parts of the vehicle. Bushnell (1990) supplies background, references and speculations on the triggering mechanisms associated with such disturbances.

Receptivity phenomena for supersonic and hypersonic boundary layers are just now beginning to receive serious attention. Whatever the receptivity mechanisms, the receptivity considerations are altered considerably by the presence of attached or bow shock waves and the fact that while vorticity and entropy disturbances are convected along streamlines, acoustic disturbances propagate along (relative) Mach lines (Morkovin 1987). Any freestream disturbance field is altered in passage through a shock wave. When entropy or vorticity disturbances on streamlines remote from the boundary layer pass through the shock wave, they are modified and are partially converted to pressure waves that impinge on the boundary layer along (relative) Mach lines (Mack 1975). Sound waves change amplitude and refract through shock waves and give rise to vorticity and entropy disturbances. Furthermore, irregularities on the vehicle surface generate pressure waves that are modified by the shock and reflected back toward the body. Once the disturbances are internalized in the boundary layer, the problem of matching wavenumbers and frequencies of amplified normal modes remains conceptually similar to that at low speeds. Very recently, Zhong (1997, 1998) calculated by DNS methods the receptivity of two-dimensional and axisymmetric hypersonic ($M = 15$) blunted configurations to freestream acoustic disturbances (upstream of the bow shock wave). He was able to show the processing of the incoming disturbances by the bow shock wave leading to vorticity, entropy as well as acoustic disturbances downstream of the shock wave, and the subsequent development of first- and second-mode disturbances in the boundary layer.

3.5.3 Roughness

While surface roughness can have a profound effect on transition, the mechanisms associated with single roughness elements are only partially understood while those responsible for transition with distributed roughness are not yet known. This has led to a large body of empirical information in the literature that is not fully consistent. These correlations are

generally based on 2D parameters such as Re_k, k/δ^*, k/δ whereas the distributed roughness is inherently 3D. The three dimensionality is introduced into the correlations by providing separate curves for each 3D shape and distribution. Nevertheless, these correlations are still the operative database for dealing with distributed roughness. The Re_θ/M_e correlations that are so prevalent in reentry vehicle transition work are now understood to be primarily a reflection of surface roughness effects.

The bulk of applicable roughness data for hypersonic vehicles comes from wind-tunnel and flight tests of the Shuttle orbiter vehicle. The roughness on this vehicle is principally from the gaps and grooves between the tiles of the thermal protection system (TPS). The prime applicable correlations are due to Bertin et al. (1982). These correlations have been recently reviewed and revised (Bouslog et al. 1997). The latest versions show good collapse of the wind-tunnel data. The flight data follow the trends of the wind-tunnel data but are about 60% higher. It is suggested that this is due to the reduced noise level in flight.

4 IMPORTANT QUESTIONS AND PRESENT POSITION OF RESEARCH

4.1 Facility and Flow-Quality Issues

Quantitative flow quality criteria for obtaining flight quality transition data in wind tunnels have only recently been enunciated (Reshotko et al. 1997) and then only for subsonic and transonic facilities. Separate criteria are given for turbulence level and for acoustic intensity.

However, transition behavior in conventional supersonic wind tunnels above $M = 2$ is dominantly due to the noise radiated onto the model from the turbulent boundary layers on the tunnel walls (Pate and Schueler 1969). This was confirmed by the important flight experiments of Dougherty and Fisher (1980). Their transition cone model had already been run in many transonic and supersonic wind tunnels throughout the world. In wind tunnels for $M > 2$ they consistently obtained the familiar "transition bucket" with a minimum Re_{tr} between Mach numbers 4 and 5. However, in flight experiments with the cone model mounted ahead of the fuselage of an F-15 aircraft, the transition Reynolds number corrected to adiabatic wall conditions showed consistent increase with Mach number over the entire flight speed range, whereas the values for Re_{tr} obtained in conventional wind tunnels started falling at $M >$ 1.6. This further accentuates the need for further flight experiments and for studies in "quiet" supersonic wind tunnels.

How does one define a "quiet" tunnel? Seemingly it should be one where the frequency bands of unstable modes are not excited by acoustic radiation from the turbulent boundary layers on the tunnel walls. "Conventional" quiet tunnels do this by maintaining laminar boundary layers on the tunnel walls (see Beckwith and Chen 1989). At $M > 8$, even conventional tunnels with turbulent sidewalls display some quiet behavior as the instability bands tend to be separated from the tunnel noise spectrum (Fig. 18). However, while the primary instability may be noise free, subharmonics may not be, and so the transition process beyond primary instability can be affected by the tunnel noise. This issue merits further study. Conventional supersonic tunnels may still be used for TS, swept attachment-line and crossflow instability studies, provided that it is ascertained that the results are not affected by tunnel noise. Additional material on this topic is contained in Reed et al. (1997).

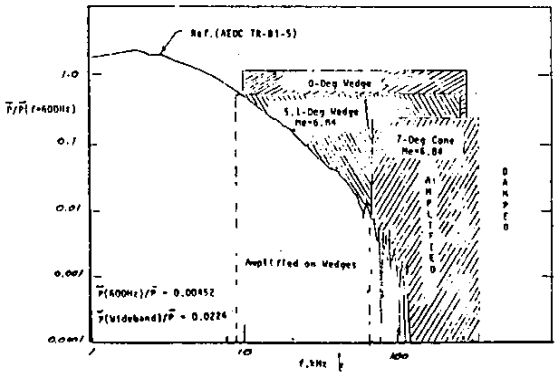

Figure 18. Tunnel B Turbulence (Acoustic) Spectrum for Mach No. 8 Nozzle, $Re/\mathrm{ft} = 3\times10^6$.

4.2 Guidelines for conducting experiments

The standards for research quality experiments on stability and transition are the "guidelines" as formulated by the U.S. Boundary Layer Transition Study Group (Reshotko 1976):

1 Any effects specifically and only associated with the test facility characteristics must be identified and if possible avoided.

2 Attention must be given to disturbances introduced by the model surface, model material and internal structure. Experimental studies should include documentation of these various factors.

3 Details of coupling of disturbances of various kinds to the boundary layer must be understood theoretically and experimentally, so that the sensitivity of the transition process to the flight environment might be determined.

4 Whenever possible, tests should involve more than one facility. Tests should have ranges of overlapping parameters, and whenever possible, experiments should have redundancy in transition measurements.

Morkovin has suggested strongly that Guideline Number Four be applied also to computational studies.

The above guidelines apply as well to flight experiments. Their implementation for flight experiments requires special attention to a number of factors:

1 The measurement of disturbance environment must be incorporated into the model design and in fact must be part of the model.

2 Attention has to be given to the maintenance and monitoring of test conditions such as Mach number, Reynolds number, angle of attack, yaw angle and surface temperature for the duration of the measurement period.

3 Attention has to be given to the maintenance and monitoring of model surface conditions for each flight. This includes protection of the model surface before launch, and recovery of the vehicle for inspection and reconditioning of the surface prior to the succeeding flight.

4 Because stability phenomena at supersonic and hypersonic speeds occur at frequencies of hundreds of kHz and even to MHz levels, there is a need for very high data sampling rates, especially when monitoring multiple channels. This poses special problems in data acquisition and data reduction. Reliable digital telemetering of data from the vehicle may also be necessary in order to minimize weight and volume of the data acquisition equipment.

4.3 Transition prediction or estimation

One can dream about an eventual capability of computing the full flowfield about a vehicle or vehicle component including the transition process. Since transition is the result of unsteady phenomena as discussed in this article, the computation through transition requires time-accurate solutions of the compressible, three-dimensional, unsteady Navier-Stokes equations in a domain large enough to contain the complete phenomenon, and with a grid that is fine enough over the extended boundary layer to capture the detailed linear eigenfunctions and the subsequent nonlinearities. In addition, initial and boundary conditions must be properly specified and enforced. The initial and upstream boundary conditions should represent properly the physical disturbance environment to which the flow is subjected. Truncation error and round-off introduce disturbances whose spectrum is non-physical. The downstream boundary condition should be non-reflecting in order that spurious feedback phenomena be absent. Herbert (1994), Reed (1994), and Reed et al. (1998) present critical discussions of the relevant issues.

At present, these requirements are marginally attainable only for small portions of simple flows. The calculation of a full vehicle is still a number of computer generations ahead of us. Parallelization of the codes and running them in parallel on multiprocessors can enable the implementation of such calculations. But until the overall capability is available, the estimation of transition locations will probably have to depend on linear stability properties of the calculated laminar flows and their synthesis into an e^N procedure that properly accounts for the three-dimensionality of the flow and the disturbances as well as for surface curvature effects.

4.4 Design considerations for hypersonic flight

Vehicle design often starts by choosing a configuration based on inviscid reasoning and then fine tuning that configuration to optimize its features. For flight up to $M = 3$, this generally means reducing form drag, wave drag, and friction drag as well as improving the low-speed high-lift properties of the configuration. Above $M = 3$, as flight Mach numbers increase, reducing aerodynamic heating loads becomes the primary consideration. Every attempt is made to minimize the need for active cooling. This means giving very definite attention to delaying transition and taking advantage of passive cooling through radiation from the aerodynamically heated surfaces to the surroundings. Rarely does this alter the original general shape of the configuration.

An exception is the recent experience with NASP - the U.S. National AeroSpace Plane (Eiswirth and Lau 1997). This is a case where the baseline configuration was axisymmetric. The forebody served as the compression surface of the inlet and was subject to adverse pressure gradient, Görtler instability and crossflow instability when the body was at angle of attack. Because of the axial symmetry, the entropy layer became successively thinner with distance downstream so that the boundary layer edge conditions were beyond swallowing and subject to second and higher mode instabilities. All of these factors promote earlier transition. In this situation, the TS as well as the Görtler and crossflow instabilities are not ameliorated by surface cooling. By the time of the configuration development, it had already been established in the NASA-Langley Quiet Pilot Tunnel that flat plates (2D) had higher transition Reynolds numbers than cones at the same freestream conditions (Chen and Malik 1988). This had also been verified by e^N calculations (Mack 1987, Elias and Eiswirth 1990).

This prompted a reconsideration of the geometry of the vehicle. The forebody was replaced by a wedge-like configuration with rounded corners at its spanwise edges. The lower surface was again a compression surface but the upper surface had a slightly favorable pressure gradient. The leading edge of course had to be blunted for its own protection. The blunting was sufficient so that the boundary layers on both the lower and upper surfaces are within the entropy layer where the edge Mach numbers are low enough that first mode TS instabilities, which can be controlled by surface cooling, are dominant. The upper surface could be radiation cooled over the flight range while the lower surface required active cooling through heat exchange with the cryofuel. Crossflow instabilities were confined to the rounded edge regions and did not add greatly to the cooling requirements. The transition behavior was verified by e^N type calculations using a 3D code known as the "e^{Malik}"code (Malik 1989, Malik and Balakumar 1992, Schwoerke 1993).

This case is instructive for future configuration development in that it shows that transition considerations could constructively alter the basic configurational shape of a vehicle.

ACKNOWLEDGEMENT

The authors would like to acknowledge the discussions and helpful suggestions of Professor Helen Reed on much of the content of this report.

REFERENCES

Adam, P.H., Hornung, H.G. 1997 Enthalpy effects on hypervelocity boundary layer transition: experiments and free flight data. *AIAA Paper 97-0764.*

Arnal, D. 1992 Boundary-layer transition: Prediction, application to drag reduction. *AGARD Rep. 786* (Special course on skin friction drag reduction).

Arnal, D. 1994 Predictions based on linear theory. *In Progress in Transition Modelling. AGARD Rep. 793.*

Arnal, D., Kufner, E., Oye, I., Tran, P. 1996 *PROGRAMME TRP TRANSITION*: Computational results for transition prediction. Study Note 7.

Arnal, D., Vignau, F., and Laburthe, F. 1991 Recent supersonic transition studies with emphasis on the swept cylinde case. *Conf. on Boundary Layer Transition and Control,* Cambridge.

Balakumar, P., Malik, M.R. 1994 Effect of adverse pressure gradient and wall cooling on instability of hypersonic boundary layers. *High Technology Corporation, Hampton, VA Rep. HTC-9404.*

Bassom, A.P., Hall, P. 1991 Vortex instabilities in three-dimensional boundary layers: the relationship between Görtler and crossflow vortices. *J. Fluid Mech. 232* pp. 647-80.

Beckwith, I.E. 1975 Development of a high-Reynolds-number quiet tunnel for transition research. *AIAA J. 13*(3) pp. 300-6.

Beckwith, I.E. Chen, F.J., Malik, M.R. 1990 Transition research in low-disturbance high-speed wind tunnels, *Laminar-Turbulent Transition III*, pp. 227-38. Eds. D. Arnal, R. Michel. Springer-Verlag.

Beckwith, I.E., Creel, T.R., Jr., Chen, F.J., Kendall, J.M. 1983 Freestream noise and transition measurements on a cone in a Mach 3.5 pilot low-disturbance tunnel. *NASA TP 2180.*

Beckwith, I.E., Malik, M.R., Chen, F.J., Bushnell, D.M. 1985 Effects of nozzle design parameters on the extent of quiet test flow at Mach 3.5. In *Laminar-Turbulent Transition.* Ed. V.V. Kozlov. New York: Springer-Verlag pp. 589-600.

Bertin, J.J., Hayden, T.E., Goodrich, W.D. 1982 Shuttle Boundary Layer Transition due to Distributed Roughness and Surface Cooling. *J. Spacecraft and Rockets. 19*(5) pp. 389-96.

Bertolotti, F.P. 1991 Compressible boundary layer stability analyzed with the PSE equations. *AIAA Paper 91-1637.*

Blanchard,A.E. 1995 *An investigation of wall-cooling effects on hypersonic boundary-layer stability in a quiet wind tunnel.* PhD Dissertation, Old Dominion University, Dept. of Mechanical Engineering, Norfolk VA.

Bouslog, S.A., Bertin, J.J., Berry, S.A., Caram, J.M. 1997 Isolated Roughness Induced Boundary Layer Transition: Shuttle Orbiter Ground Tests and Flight Experience. *AIAA Paper 97-0274.*

Bushnell, D.M. 1990 Notes on Initial Disturbance Fields for the Transition Problem. *In Instability and Transition Vol I.* Eds. Hussaini, Voight., Springer-Verlag, pp. 217-32.

Bushnell, D.M., Huffman, J.K. 1967 Investigation of heat transfer to leading edge of a 76° swept fin with and without chordwise slots and correlations of swept-leading-edge transition data for Mach 2 to 8. *NASA-TM-X-1475.*

Cattafesta, III, L.N., Iyer, V., Masad, J., King, R., Dagenhart, J. 1995 Three-dimensional boundary-layer transition on a swept wing at mach 3.5. *AIAA J. 33* (11).

Chang, C.-L., Malik, M., Erlebacher, G., Hussaini, M. 1991 Compressible stability of growing boundary layers using parabolized stability equations. *AIAA Paper 91-1636.*

Chang, C.-L., Malik, M.R. 1993 Non-parallel stability of compressible boundary layers. *AIAA Paper 93-2912.*

Chapman, G.T. 1961 Some effects of leading edge sweep on boundary-layer transition at supersonic speeds. *NASA-TN-D-1075.*

Chen, F. and Malik, M. 1988 Comparison of boundary layer transition on a cone and flat plate at Mach 3.5. *AIAA Paper 88-0411.*

Chen, F.J., Malik, M.R., Beckwith, I.E. 1985 Instabilities and transition in the wall boundary layers of low-disturbance supersonic nozzles. *AIAA Paper 85-1573.*

Chen, F-J , Malik, M.R., Beckwith, I.E. 1989 Comparison of Boundary Layer Transition on a Cone and Flat Plate at Mach 3.5. *AIAA J. 27*(6) pp. 687-93.

Creel, T.R., Beckwith I.E. and Chen, F.J. 1987 Transition on swept leading edges at Mach 3.5. *J. Aircraft 25*(10).

Cumpsty, N. and Head, M. 1967. The calculation of three-dimensional turbulent boundary layers. Part II: attachment line flow on an infinite swept wing. *Aeron. Quart., XVIII,* Part 2.

Da Costa, J.D. 1990 *Contribution à l'étude de la transition de bord d'attaque par contamination en écoulement hypersonique.* Master's thesis, Poitiers University, France.

Dagenhart, J.R. 1981 Amplified crossflow disturbances in the laminar boundary layer on swept wings with suction. *NASA TP 1902.*

Dallmann, U., Hein, S., Koch, W., Bertolotti, F., Simen, M., Stolte, A., Gordner, A., and Nies, J. 1996 Status of the theoretical work within DLR's non empirical transition prediction project. *2nd European forum on Laminar Flow Technology,* Bordeaux.

Dando, A. 1992 The inviscid compressible Görtler problem in three-dimensional boundary layers. *Theoret. Comput. Fluid Dyn. 3* pp. 253-65.

Dando, A., Seddougui, S.O. 1991 The inviscid compressible Görtler problem. *ICASE Rep. 91-54.*

de Luca, L., Cardone, D. Aymer de la Chevalerie, D. Fonteneau, A. 1993 Görtler instability of a hypersonic boundary layer. *Exp. Fluids 6* 10-6.

Doggett, G.P., Chokani, N., Wilkinson, S.P. 1997 Effect of angle of attack on hypersonic boundary-layer stability. *AIAA J. 35*(3) pp. 464-70.

Dougherty, N.S., Fisher, D.F. 1980 Boundary layer transition on a 10-degree cone: Wind tunnel/flight data correlation. *AIAA Paper 80-0154.*

Eiswirth, E., Lau, K 1997 Boundary Layer Transition on Hypersonic Configurations-Lessons Learned from NASP. *Private communication to E. Reshotko.*

Eiswirth, E., Lau, K. 1997 Boundary Layer Transition on Hypersonic Configurations -Lessons Learned from NASP. *AIAA Paper 97-1909.*

El-Hady, N.M. 1991 Nonparallel instability of supersonic and hypersonic boundary layers. *Phys. Fluids A 3*(9) pp. 2164.

El-Hady, N.M., Verma, A.K. 1983a Gworth of Görtler vortices in compressible boundary layers along curved surfaces. *J. Eng. Appl. Sci 2* pp. 213-38.

El-Hady, N.M., Verma, A.K. 1983b. Görtler instability of compressible boundary layers. *AIAA J. 22* pp. 1354-55.

Elias, T.I., Eiswirth, E.A. 1990 Stability Studies of Planar Transition in Supersonic Flows. *AIAA Paper 90-5233.*

Fisher, D. and Dougherty, N. 1982 Inflight transition measurements on a 10 deg. Cone at Mach numbers from 0.5 to 2. *NASA TP 1971.*

Fu, Y.B., Hall, P. 1991a Nonlinear development and secondary instability of Görtler vortices in hypersonic flows. *ICASE Rep. 91-39.*

Fu, Y.B., Hall, P. 1991b Effect of Görtler vortices, wall cooling and gas dissociation of the Rayleigh Instability in a hypersonic boundary layer. *ICASE Rep. 91-87.*

Fu, Y.B., Hall, P. 1994 Crossflow effects on the growth rate of inviscid Görtler vortices in a hypersonic boundary layer. *J. Fluid Mech. 276* 343-67.

Fu, Y.B., Hall, P. Blackaby, N. 1993 On the Görtler instability in hypersonic flows: Sutherland law fluids and real gas effects. *Phil. Trans. R. Soc. Lond. A 342* 325-77.

Gaillard, L. 1993 *Etude de la transition de bord d'attaque sur un cylindre en flèche en écoulement hypersonique.* Master's thesis, Poitiers University, France.

Gasperas, G. 1990 Stability of the laminar boundary layer for an imperfect gas. *Laminar-Turbulent Transition II.* Eds. D. Arnal, R. Michel. Berlin: Springer-Verlag. pp. 291-302.

Gaster, M. 1967 On the flow along leading edges. *Aeron. Quart, XVIII* Part 2.

Gaster, M. 1974 On the effects of boundary-layer growth on flow stability. *J. Fluid Mech. 66* pp. 465-80.

Germain, P., Cummings, E. and Hornung, H. 1993 Transition on a sharp cone at high enthalpy; new measurements in the Shock Tunnel T5 at GALCIT. *AIAA Paper 93-0343.*

Görtler, H. 1955 Dreidimensionale Instabilität der ebenen Staupunktströmung gegenüber wirbelartigen Störungen. In *Fifty Years of Boundary Layer Research.* Eds. Görtler and Tollmien. Vieweg and Sohn, Braunschweig.

Hall, P. 1985 The Görtler vortex instability mechanism in three-dimensional layers. *Proc. R. Soc. London Ser. A 399* pp. 135-52.

Hall, P., Fu, Y.B. 1989 On the Görtler vortex instability mechanism at hypersonic speeds. *Theoret. Comput. Fluid Dyn. 1* pp. 125-34.

Hall, P., Malik, M.R. 1989 The growth of Görtler vortices in compressible boundary layers. *J. Eng. Math. 23* pp. 239-45.

Hall, P., Malik, M.R., Poll, D.I.A. 1984 On the stability of an infinite swept attachment-line boundary layer. *Proc. Roy. Soc. Lond. A. 395* pp. 229-45.

Hämmerlin, G. 1955 Zur Instabilitätstheorie der ebenen Staupunktströmung. In *Fifty Years of Boundary Layer Research.* Eds. Görtler and Tollmien. Vieweg and Sohn, Brauschweig.

Hämmerlin, G. 1961 Uber die Stabilität einer kompressiblen Störmung längs einer konkaven Wand bei verschiedenen Wand-temperaturvehältnissen. *Deutsche Versuchsanstalt für Luftfahrt*, Bericht 175.

Hanifi, A. 1995 *Nonlocal stability analysis of the compressible boundary layer on a yawed cone.* Ph.D. diss., KTH, Stockholm.

Hanifi,A., Henningson, D., Hein, S., Bertolotti, F., and Simen, M. 1994 Linear nonlocal instability analysis the linear NOLOT code. *FFA Rep. 1994-54.*

Herbert, Th. 1988 Secondary instability of boundary layers. *Ann. Rev. Fluid Mech. 20* pp. 487-526.

Herbert, Th. 1994 Parabolized stability equations. In *Progress in Transition Modelling. AGARD-FDP VKI Course. Rep. 793.* Ed. W. S. Saric.

Herbert, Th., Esfahanian, V. 1992 Stability of hypersonic flow over a blunt body. *AGARD CP 514 Theoretical and Experimental Methods in Hypersonic Flows.*

Holden, M.S., Bower, D.R., Chadwick, K.M. 1995 Measurements of boundary layer transition on cones at angle of attack for Mach numbers from 11 to 13. *AIAA Paper No. 95-2294.*

Holden, M.S., Chadwick, K.M. 1995 Studies of laminar, transitional, and turbulent hypersonic flows over curved compression surfaces. *AIAA Paper 95-0093.*

Holden, M.S., Kolly, J.M. 1995 Attachment-line transition studies on swept cylindrical leading edges at Mach numbers from 10-12. *AIAA Paper 95-2279.*

Holden, M.S., Kolly, J.M., Bower, D. 1994 Attachment-line transition studies on swept cylindrical leading edges at Mach numbers from 10-12. *CALSPAN Tech. Rep. 26106.*

Howarth, L. 1948 Concerning the effect of compressibility on laminar boundary layers and their separation. Proceedings of the *Royal Society of London A. Vol. 194.*

Illingworth, C.R. Steady flow in the laminar boundary layer of a gas. . *Proc. R. Soc. London Ser. A Vo. 199.*

Jallade, S., Arnal, D., Ha Minh, H. 1990 Theoretical study of Görtler vortices; linear stability approach. In *Laminar-Turbulent Transition.* Eds. D. Arnal, R. Michel. Berlin: Springer-Verlag. pp. 563-72.

Johnson, C., Stainback, P., Wiker, K., and Bony, L. 1972 Boundary layer edge conditions and transition Reynolds number data for a flight test at Mach 20 (Reentry-F). *NASA TM X2584.*

Johnson, H.B., Candler, G.V., Hudson, M.L. 1997 Numerical Study of Hypersonic Boundary Layer Transition on a Blunt Body. *AIAA Paper 97-0554.*

Kendall, J.M. 1975 Wind tunnel experiments relating to supersonic and hypersonic boundary-layer transition. *AIAA J. 13*(3) pp. 290-9.

Kimmel R.L., Demetriades, A., Donaldson, J. 1996 Space-time correlation measurements in a hypersonic transitional boundary layer. *AIAA J. 34*(12) pp. 2484-9.

Kimmel, R.L., Poggie, J. 1997 Disturbance evolution and breakdown to turbulence in a hypersonic boundary layer: ensemble-averaged structure. *AIAA Paper 97-0555.*

King, R.A. 1991 Mach 3.5 boundary layer transition on a cone at angle of attack. *AIAA Paper 91-1804.*

Klebanoff, P.S., Tidstrom, K.D., Sargent, L.M. 1962 Three-dimensional nature of boundary layer instability. *J. Fluid Mech. 12* pp. 1-34.

Kobayashi, R., Kohama, Y. 1977 Taylor-Görtler instability of compressible boundary layers. *AIAA J. 15* pp. 1723-7.

Krogmann, P. 1977 An experimental study of boundary layer transition on a slender cone at Mach 5. *AGARD-CP-224.*

Krogmann, P. 1996 *Private communication to W.S. Saric, 26 Nov. 1996.*

Lachowitz, J.T., Chokani, N., Wilkinson, S.P. 1996 Boundary-layer stability measurements in a hypersonic quiet tunnel. *AIAA J. 34*(12) pp. 2496-500.

Lees, L., Lin, C.C. 1946 Investigation of the stability of the laminar boundary layer in a compressible fluid. *NACA TN 1115.*

Mack, L.M. 1965a Computation of the stability of the laminar compressible boundary layer. In *Methods in Comp. Phys. Vol. 4* pp. 247-99. Ed. B. Alder. Academic Press, New York.

Mack, L.M. 1965b The stability of the compressible laminar boundary layer according to a direct numerical solution. *AGARDograph 97*, pt.1 pp. 329-62.

Mack, L.M. 1969 Boundary layer stability theory. *JPL Rep. 900-277, Rev. A.*

Mack, L.M. 1975 Linear stability theory and the problem of supersonic boundary-layer transition. *AIAA J. 3* pp. 278-89.

Mack, L.M. 1984 Boundary-layer linear stability theory. *AGARD Rep. 709* (Special course on stability and transition of laminar flows).

Mack, L.M. 1987 Stability of Axisymmetric Boundary Layers on sharp Cones at Hypersonic Mach Numbers. *AIAA Paper 87-1413.*

Mack, L.M. 1990a On the inviscid acoustic-mode instability of supersonic shear flows, Part 1: two-dimensional waves. *J. Theor. and Comp. Fluid Dyn. 2* pp. 97-123.

Mack, L.M. 1990b *Private communication to E. Reshotko.*

Malik, M. 1990a Numerical methods for hypersonic boundary layer stability. *J. Comp. Phys. 86* pp.376-423.

Malik, M., Balakumar, P. 1992 Instability and transition in threedimensional supersonic boundary layers. *AIAA Paper 92-5049.*

Malik, M.R. 1984 Instability and transition in supersonic boundary layers. In *Laminar Turbulent Boundary Layers.* Energy Sources Technology Conference, New Orleans.

Malik, M.R. 1988 Stability theory for NASP transition prediction. *Fifth National Aero-Space Plane Symposium,* Paper 57.

Malik, M.R. 1989a Prediction and control of transition in supersonic and hypersonic boundary layers. *AIAA J. 27*(11) pp. 1487-93.

Malik, M.R. 1989b e^{Malik} : A New Spatial Stability Analysis Program for Transition Prediction Using the e^N Method. *High Technology Rep. HTC-8902.*

Malik, M.R., Beckwith, I.E. 1988 Stability of a supersonic boundary layer along a swept leading edge. *AGARD CP 438.*

Malik, M.R., Spall, R.E., Chang, C.L. 1990a Effect of nose bluntness on boundary layer stability and transition. *AIAA Paper 90-0112.*

Malik, M.R., Zang, T., Bushnell, D.M. 1990b Boundary layer transition in hypersonic flows. *AIAA Paper 90-5232.*

Morkovin, M.V. 1969 Critical evaluation of transition from laminar to turbulent shear layers with emphasis on hypersonically traveling bodies. *Air Force Flight Dynamics Laboratory Rep. AFFDL-TR-68-149.*

Morkovin, M.V. 1969 On the many faces of transition. *Viscous Drag Reduction.* Ed. C.S. Wells, Plenum.

Morkovin, M.V. 1987 Transition at hypersonic speeds. *ICASE Interim Report 1 (NASA Contractor Rep. 178315).*

Morkovin, M.V. 1988 Recent insights into instability and transition to turbulence in open-flow systems. *AIM Paper 88-3675.* Also *ICASE Report No. 88-44, (NASA Contractor Report 181693).*

Morkovin, M.V., Reshotko, E. 1990 Dialogue on progress and issues in stability and transition research. *Laminar-Turbulent Transition III.* Eds. D. Arnal, R. Michel. pp. 3-30. Berlin: Springer-Verlag.

Morrisette, E. 1976 Roughness induced transition criteria for space shuttle-type vehicles. *J. Aircraft, 13*(2).

Murakami, A., Stanewsky, E., Krogmann, P. 1995 Boundary layer transition on swept cylinders at hypersonic speeds. *AIAA Paper 95-2276.*

Pate, S.R. 1978 Dominance of radiated aerodynamic noise on boundary-layer transition in supersonic-hypersonic wind tunnels: theory and application. *AEDC-TR-77-107.*

Pate, S.R., Schueler, C.J. 1969 Radiated aerodynamics noise effects on boundary-layer transition in supersonic and hypersonic wind tunnels. *AIAA J. 7* pp. 450-7.

Pfenninger, W. 1965 Some results from the X-21 program. Part I. Flow phenomenon at the leading edge of swept wings. *AGARDograph No. 97.*

Pfenninger, W. 1977 Laminar Flow control Laminarization.. *AGARD Rep. R-654.* (Special course: concepts in drag reduction).

Pfenninger, W. and Bacon, Jr, J.W. 1969. Amplified laminar boundary layer oscillations and transition at the front attachment line of a 45 deg. swept flat_nosed wing with and without boundary-layer suction. In *Viscous Drag Reduction.* Ed. C. Wells. Plenum Press.

Poggie, J., Kimmel, R.L. 1997 Disturbance evolution and breakdown to turbulence in a hypersonic boundary layer: instantaneous structure. *AIAA Paper 97-0556.*

Poll, D. 1978 Some aspects of the flow near a swept attachment line with particular reference to boundary layer transition. *Cranfield College of Aeronautics Tech. Rep. 7805.*

Poll, D. 1985 Boundary layer transtion on the windward face of space shuttle during reentry. *AIAA Paper 85-0899.*

Poll, D.I.A. 1984 Transition Description and Prediction in Three-Dimensional Flows, *AGARD Rep. 709.* (Special course: stability and transition of laminar flows).

Poll, D.I.A. 1985 Some observations of the transition process on the windward face of a long yawed cylinder. *J. Fluid Mech. 150.*

Poll, D.I.A. 1986 A new hypothesis for transition on the windward face of space shuttle. *J. Space. Rockets, 23*(6).

Potter, J.L. 1974 *The unit Reynolds number effect on boundary layer transition.* Ph.D. Dissert. Vanderbilt Univ.

Potter, J.L. 1980 Review of the influence of cooled walls on boundary-layer transition. *AIAA J. 18*(8) pp. 1010-2.

Radeztsky, R.H. Jr., Reibert, M.S., Saric, W.S., Takagi, S. 1993 Effect of micron-sized roughness on transition in swept-wing flows. *AIAA Paper 93-0076.*

Reed, H.L. 1994 Direct Numerical Simulation of Transition: The Spatial Approach. In *Progress in Transition Modelling. AGARD-FDP VKI Course. Rep. 793.* Ed. W.S. Saric.

Reed, H.L., Haynes, T.S. 1994 Transition correlations in three-dimensional boundary layers. *AIAA J. 32*(5) pp. 923-9.

Reed, H.L., Haynes, T.S., Saric, W.S. 1998 Computational Fluid Dynamics Validation Issues in Transition Modeling. *AIAA J. 36*(5) pp. 742-51.

Reed, H.L., Kimmel, R.L., Schneider, S.P., Arnal, D. 1997 Drag prediction and transition in hypersonic flow. *AIAA Paper 97-1818* (also *AGARD-CP-600, Vol. 3* pp. C15-1-17).

Reed, H.L., Saric W.S. 1989 Stability of three-dimensional boundary layers. *Ann. Rev. Fluid Mech. 21* pp. 235-84.

Reed, H.L., Saric, W.S., Arnal, D. 1996 Linear stability theory applied to boundary layers. *Annu. Rev. Fluid Mech. 28* pp. 389-428.

Reshotko, E, Saric, W.S., Nagib, H.M. 1997 Flow Quality Issues for Large Wind Tunnels. *AIAA Paper 97-0225.*

Reshotko, E. 1969 Stability Theory as a Guide to the Evaluation of Transition Data. *AIAA J. 7*(6) pp. 1086-91.

Reshotko, E. 1986 Stability and Transition: what do we know? *Proc. U.S. Nat;l. Congress Appl. Mech.* Austin, TX. ASME, 421.

Reshotko, E. 1994 Boundary layer instability, transition, and control. *AIAA Paper. 94-0001.*

Reshotko, E. Khan, M.M.S. 1980 Stability of the laminar boundary layer on a blunted plate in supersonic flow. In *Laminar Turbulent Transition I*, Springer-Verlag.

Reshotko, E., Beckwith, I. 1958 Compressible laminar boundary layer over a yawed infinite cylinder with heat transfer and arbitrary Prandtl number. *NACA Tech. Rep. 1379.*

Saric, W.S. 1994a Physical description of boundary-layer transition: experimental evidence. In *Progress in Transition Modelling. AGARD-FDP VKI Course. Rep. 793.* Ed. W.S. Saric

Saric, W.S. 1994b Görtler vortices. *Ann. Rev. Fluid Mech.* **26** pp. 379-409.

Schneider, S.P., Haven, C.E. 1995 Quiet flow Ludwieg tube for high-speed transition research. *AIAA J. 33*(4) pp. 688-93.

Schwoerke, S. 1993 Quiet Tunnel Results and Analysis for Various Forebody Shapes at Mach 3.5. *National Aero-Space Plane Technology Review, Paper No. 158.*

Simen, M., Dallmann, U. 1992 On the instability of hypersonic flow past a pointed cone: Comparison of theoretical and experimental results at Mach 8. *DLR-FB 92-02. AGARD CP 514 Theoretical and Experimental Methods in Hypersonic Flows.*

Skuratov, A., Fedorov, A. 1991 The laminar-turbulent transition past roughness at the attachment line of a swept cylinder in supersonic flow. *Izv. AN SSSR, Mekh. Zhidk. I Gasa (translated in english),* (6) pp. 2835.

Smith, A.M.0., Gamberoni, N. 1956 Transition, pressure gradient and stability theory. *DAC Report No. ES 26388.*

Spalart, P.R. 1989 Direct numerical study of leading-edge contamination. *AGARD-CP 438.*

Spall, R.E., Malik, M.R. 1989 Görtler vortices in supersonic and hypersonic boundary layers. *Phys. Fluids A 1* pp. 1822-35.

Stetson, K.F. 1982 Mach 6 experiments of transition on a cone at angle of attack. *J. Spacecraft Rockets* **19** (5) pp. 397-403.

Stetson, K.F., Kimmel, R.L. 1992 On hypersonic boundary-layer stability. *AIAA Paper 92-0737.*

Stetson, K.F., Kimmel, R.L., Thompson, E.R., Donaldson, J.C., Siler, L.G., 1991 A Comparison of planar and conical boundary layer stability and transition at a Mach number of 8. *AIAA Paper 91-1639.*

Stetson, K.F., Thompson, E.R., Donaldson, J.C., Siler, L.G. 1984 Laminar boundary layer stability experiments on a cone at Mach 8, Part 2: blunt cone. *AIAA Paper 84-0006.*

Stewartson, K. Correlated Compressible and Incompressible boundary Layers. *Proc. R. Soc. London Ser. A Vol. 200* pp. 84-100.

Stuart, J.T. 1984 Instability of laminar flows, nonlinear growth of fluctuations and transition to turbulence. *In Turbulence and Chaotic Phenomena in Fluids, Ed. T. Tatsumi.* Amsterdam: North-Holland pp. 17-26.

Stuckert, G.K. 1991 *Linear stability theory of hypersonic, chemically reacting viscous flows.* Ph.D. Dissert., Ariz. State Univ., Tempe.

Stuckert, G.K., Reed, H.L. 1994 Linear disturbances in hypersonic, chemically reacting shock layers. *AIAA J. 32*(7) pp. 1384-93.

Tran, P., Seraudie, A., Wendt, V., and Poll, D.I.A. 1995 *PROGRAMME TRP TRANSITION* : Experimental results for transition prediction. Study Note 6.

Tumin, A.M., Chernov, Yu. P. 1988 Asymptotic analysis of flow instability in a compressible boundary layer on curved surface. *Ah. Prikl. Mekh. Tekh. Fiz. 3* pp. 84-9.

Van Ingen, J.L. 1956 A suggested semi-empirical method for the calculation of the boundary-layer transition region. *Rep. No. VTH 71 and 74*, Dept. Aero. Eng., Tech. Univ. Delft, Neth.

Wendt, V., Kreplin, H., Höhler, G., Grosche, F., Krogmann, P., Simen, M. 1993 Planar and conical boundary layer stability experiments at Mach 5. *AIAA Paper 93-5112.*

Wendt, V., Simen, M., Hanifi, A. 1995 An experimental and theoretical investigation of instabilities in hypersonic flat plate boundary layer flow. *Phys. Fluids 7*(4) pp. 877-87.

Wilkinson, S. 1997 A Review of Hypersonic Boundary Layer Stability Experiments in a Quiet Mach 6 Wind Tunnel. *AIAA Paper 97-1819.*

Wright, R.L., Zoby, E.V. 1977 Flight boundary layer transition measurements on a slender cone at Mach 20. *AIAA Paper 77-719.*

Zhong, X. 1997 Direct Numerical Simulation of Hypersonic Boundary-Layer Transition over Blunt Leading Edges Part II: Receptivity to Sound. *AIAA Paper 97-0756.*

Zhong, X. 1998 Direct Numerical Simulation of 3-D Hypersonic boundary Layer Receptivity to Freestream Disturbances. *AIAA Paper 98-0533.*